

Hybrid lunar ISRU plant: a comparative analysis with carbothermal reduction and water extraction

Kosuke Ikeya^{a,*}, Francisco J. Guerrero-Gonzalez^b, Luca Kiewiet^c, Michel-Alexandre Cardin^d, Jan Cilliers^a, Stanley Starr^a and Kathryn Hadler^e

^aDepartment of Earth Science and Engineering, Imperial College London, Prince Consort Road, London, SW7 2AZ, The United Kingdom

^bProfessorship of Lunar and Planetary Exploration, Technical University of Munich, Lise-Meitner-Str. 9, Ottobrunn, 85521, Germany

^cInstitute of Space Systems, German Aerospace Center, Robert-Hooke-Straße 7, Bremen, 28359, Germany

^dDyson School of Design Engineering, Imperial College London, Imperial College Road, London, SW7 2DB, United Kingdom

^eEuropean Space Resources Innovation Centre (ESRIC), Luxembourg Institute of Science and Technology (LIST), 5 Avenue des Hauts-Fourneaux, L-4362, Luxembourg

ARTICLE INFO

Keywords:

in-situ resource utilization
lunar regolith
oxygen extraction
carbothermal reduction
icy regolith
uncertainty analysis

ABSTRACT

To establish a self-sustained human presence in space and to explore deeper into the solar system, extensive research has been conducted on In-Situ Resource Utilization (ISRU) systems. Past studies have proposed and researched many technologies to produce oxygen from regolith, such as carbothermal reduction and water extraction from icy regolith, to utilize it for astronauts' life support and as the propellant of space systems. However, determining the most promising technology remains challenging due to uncertainties in the lunar environment and processing methods. To better understand the lunar environment and ISRU operations, it is crucial to gather more information. Motivated by this need for information gathering, this paper proposes a new ISRU plant architecture integrating carbothermal reduction of dry regolith and water extraction from icy regolith. Two different hybrid plant architectures integrating both technologies (1) in parallel and (2) in series are examined. The former involves mining and processing in both a Permanently Shadowed Region (PSR) and a peak of eternal light in parallel, while the latter solely mines in a PSR. In this series hybrid architecture, the dry regolith tailings from water extraction are further processed by carbothermal reduction. This paper conducts a comparative analysis of the landed mass and required power of each plant architecture utilizing subsystem-level models. Furthermore, based on uncertain parameters such as resource content in regolith, the potential performance range of each plant was discovered through Monte Carlo simulations. The result indicates the benefit of the series hybrid architecture in terms of regolith excavation rate, while its mass cost seems the highest among the studied architectures.


1. Introduction

In-Situ Resource Utilization (ISRU), also known as Space Resource Utilization (SRU), aims to process and utilize local extraterrestrial resources to enable long-term human presence beyond low Earth orbit. Resources on our nearest planetary bodies, i.e., the Moon and Mars, include water in the form of ice or hydrated minerals [1–3], atmospheric carbon dioxide [2], and regolith, which is a source of oxygen and metals [1, 3]. These resources can be processed by a variety of thermo- and electrochemical techniques [2, 4] to produce life support consumables (e.g., H₂O, O₂), rocket fuel propellant (e.g., CH₄, H₂, O₂), or infrastructure and spare parts (e.g., regolith, metals). Among various ISRU activities, lunar ISRU has been increasingly gathering a large amount of attention in response to the concurrent Artemis program and other initiatives of going back to the Moon.

For lunar ISRU, several architectures for the production of these propellant and life-support consumables have been considered: (1) oxygen extraction from dry-regolith processing with reducing agents, such as hydrogen [5, 6] and methane [7–11], (2) oxygen extraction via electrolysis of molten regolith [12] and in molten salt [13, 14], and (3) hydrogen and oxygen extraction from lunar icy regolith [15–24]. Choosing the most suitable architecture is crucial for successful and economically viable lunar ISRU [3, 4, 25]. However, it is highly unpredictable if either architecture would perform significantly better than the other due to uncertainties in the resource and operation. Building an ISRU plant dedicated to only one of these technologies might be suboptimal when these inherent uncertainties unfold.

Recognizing uncertainty, this paper proposes a novel architecture: a hybrid ISRU plant, where liquid oxygen (LOX) and liquid hydrogen (LH₂) are coproduced from both dry and icy regolith on the Moon. Hybrid architectures that utilize multiple resources simultaneously have previously been proposed only for Mars ISRU [26, 27]; the benefits and

*Corresponding author

 k.ikeya22@imperial.ac.uk (K. Ikeya)

 <https://profiles.imperial.ac.uk/k.ikeya22> (K. Ikeya)

ORCID(s): 0000-0003-1172-1527 (K. Ikeya)

costs of processing both dry and icy regolith on the Moon have not been thoroughly explored.

Two different types of hybrid lunar ISRU architectures are proposed. In the first architecture, carbothermal reduction and direct water extraction from icy regolith occur simultaneously in parallel. In the other architecture, these two processes are integrated in series, i.e., the remaining dry regolith after water extraction is further processed through carbothermal reduction. The Concept of Operations (ConOps) suitable for each architecture is carefully defined. Although these proposed hybrid architectures add complexity to the overall system, they can mitigate the risk of failure by avoiding reliance on a single extraction technology.

This paper further compares the mass and power budgets, along with other system performance indicators, of the proposed hybrid plant architecture with single technology architectures: carbothermal reduction of dry regolith and direct water extraction from icy regolith. A holistic and multidisciplinary approach that models end-to-end ISRU production plants is utilized to understand the benefits and drawbacks of specific technologies and processing techniques [28].

Although there have been an increasing number of missions to the Moon and studies about it [29], the knowledge available about the lunar environment still contains large uncertainty [30]. The effects of this uncertainty on the performance of a plant and its operation have not been discussed enough [31]. Therefore, to examine the performance of these different plant architectures in various conditions, Monte Carlo simulations explicitly address resource and operational uncertainty. The results highlight the benefits and drawbacks inherent to each plant design.

The rest of the paper is organized as follows: Section 2 summarizes past studies in hybrid ISRU architectures, mass and power estimation of ISRU systems, and uncertainty related to lunar ISRU highlighting the research gap addressed by this paper. Section 3 introduces the hybrid ISRU production plant concept, including assumptions made and ConOps. In Section 4, the modeling approach of this work for the mass and power estimations is explained. The results of the mass and power estimations are discussed further in Section 5. Section 6 introduces the intrinsic uncertainty of the lunar environment and ISRU systems, and its effects on the performance of each ISRU plant operation. Section 7 discusses the potential benefits and risks of each plant design as well as critical parameters affecting the performance

significantly. Finally, concluding remarks are outlined in Section 8.

2. Background and related Work

2.1. Hybrid ISRU architecture

Compared to the conventional single-technology ISRU architectures, hybrid architectures combining multiple process technologies have not been well-researched. Kleinhenz and Paz [26] proposed the idea of utilizing the Martian atmosphere and subsurface water ice simultaneously for Mars ISRU. This study revealed a potential reduction in landed mass compared to the conventional oxygen production architecture for Mars return vehicle propellant by producing both liquid methane and liquid oxygen.

Chen et al. [27] also showed the benefit of employing both hydrogen reduction and water extraction from Martian soil through the optimization of technology selection in terms of crewed Mars mission cost. Even though this study showed the economic benefit, they also noted the potential increase in the complexity of its development, deployment, and operation.

While it is likely that these hybrid architectures add significant complexity, these past studies indicate some potential benefits. These drawbacks and advantages require more in-depth analyses to fully assess these architectures compared to other ISRU options. Lunar ISRU utilizing both dry and icy regolith, especially, needs more understanding given the increasing international interest in human lunar exploration. However, the performance of hybrid lunar ISRU is yet to be researched.

2.2. Mass and power estimation for ISRU

The estimation of mass and power budgets of all the necessary subsystems is essential before considering ISRU as a viable alternative to transporting all material resources from Earth [32]. Therefore, the estimation has been conducted extensively through (mainly) computer modeling with different fidelity levels.

As an example of relatively low-fidelity modeling, Chen et al. [27] developed a database of subsystem-level specific masses and powers based on literature, such as Ref. [33], and integrated it into an Earth-Moon-Mars space resources logistics network. This approach analyzed the effect of ISRU deployment location (i.e., the Moon or a near-Earth object) regarding system mass and monetary mission cost.

While these models can capture the trend in mass and power for different architectures, they often overlook the

detailed ConOps, potentially missing some key subsystems and components to be considered. Recently, more detailed models considering ConOps carefully have been developed. Linne et al. [7] modeled in detail the extraction of oxygen via carbothermal reduction of dry regolith to identify the feasibility of deploying such a plant considering the capacity of a lunar lander. Guerrero-Gonzalez and Zabel [32] also accounted for metal processing by comparing three different ISRU techniques, hydrogen reduction, molten regolith electrolysis, and molten salt electrolysis, and estimating the mass and required power of each subsystem. Kiewiet et al. [22] modeled water extraction from icy regolith via three different heating methods and conducted a trade-off study. Kleinhenz and Paz [23] compared the system mass and power of two different architectures: the extraction of both H_2 and O_2 from water ice in the lunar southern polar region and solely O_2 based on the work developed by Linne et al. [7].

2.3. Recognizing uncertainty in ISRU

Although the studies in Section 2.2 aimed to quantitatively analyze the most promising ISRU technologies, it should be noted that the comparisons made in them are based on deterministic assumptions for some key parameters such as resource or operational availability. However, as Cilliers et al. [30] showed by considering uncertainty in many aspects, such as resource content, such oversimplification by ignoring the uncertainty of key parameters might change the requirements for the ConOps and, therefore, overlooks the potential risk of underperformance. Takubo et al. [34] considered the uncertainty in the water production rate and the yearly decay rate in this production. Although the work successfully integrated these parameters into a spaceflight campaign design, the uncertainty recognized in this work is limited. Malone et al. [35] also recognized uncertainty in the entire mining process, such as potential subsystem technological malfunction and power generation. Their study integrated the recognized uncertainty into a Comprehensive Lunar Mining Simulator to help decision-makers through a serious game approach.

None of these studies have compared different ISRU technologies considering the effect of the uncertain lunar environment and ISRU operations. Due to the large difference between dry and icy regolith processing, potential benefits and risks can be easily overlooked when ignoring the uncertainty. Inspired by Ref. [30], this paper models the distributions of uncertain parameters and examines their

effects on plant performance indicators such as regolith excavation rate.

3. Hybrid lunar ISRU plant concept

This section first proposes two different hybrid lunar ISRU architectures. Technologies selected for further analyses and the detailed ConOps are explained in Sec. 3.2 and 3.3, respectively.

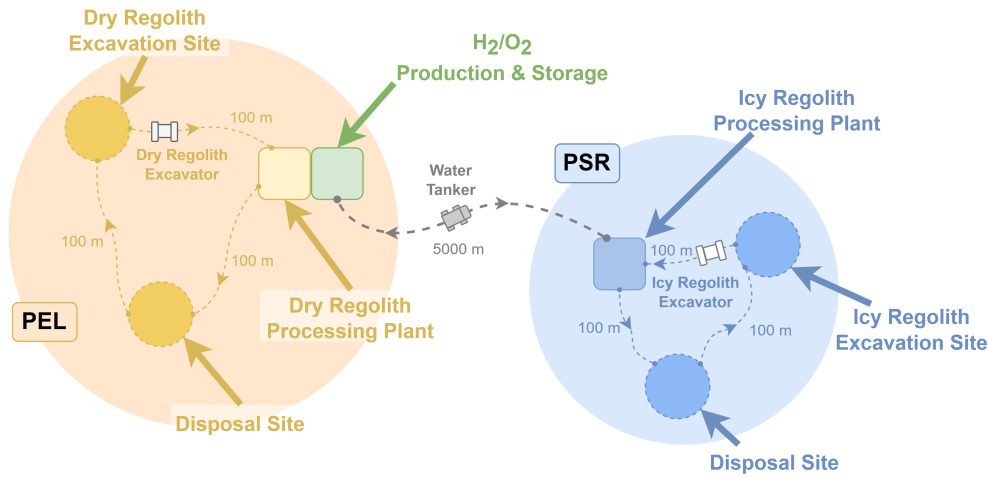
3.1. Overview and assumptions

The lunar South Pole was selected as an ideal location to place the hybrid ISRU production plant due to the increasing evidence of volatile and water ice presence in its Permanently Shadowed Regions (PSRs) [36–38] and the existence of Peaks of Eternal Light (PELs) that provide extended periods of solar illumination [39, 40].

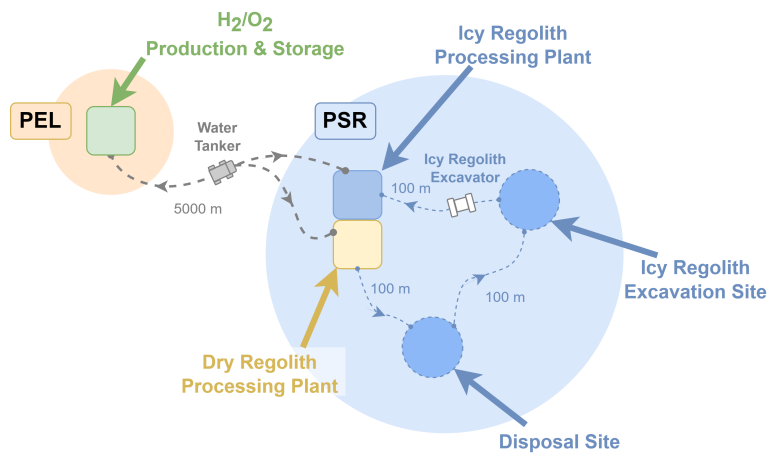
Two different types of hybrid production plants are considered in this paper. The first architecture considered is a Parallel Hybrid plant that excavates and extracts resources from both PEL and PSR sites (Fig. 1a). In the PEL, dry regolith is excavated and processed to extract oxygen. Simultaneously in the PSR, water is extracted from icy regolith. The extracted water is transported from the PSR to the PEL by a mobile water transportation solution, where the water is then electrolyzed into O_2 and H_2 . This concept is based on the water extraction plant design proposed by Kleinhenz and Paz [23]. Thermochemical extraction processes, such as carbothermal or hydrogen reduction of dry regolith, produce water as an intermediate product, and therefore, water electrolysis and storage of oxygen and hydrogen can be shared between dry and icy regolith processing.

The second architecture considered is a Series Hybrid, where dry regolith tailings from the water extraction of icy regolith are further processed directly in the PSR (Fig. 1b). This architecture can potentially maximize the oxygen and hydrogen yield from the regolith feedstock by utilizing both water ice and lunar regolith from excavated feedstock. Similar to the Parallel Hybrid architecture, the extracted and produced water is transported to a PEL for further processing. The detailed ConOps of both hybrid plants are further described in Section 3.3.

Another possibility would be targeting micro cold traps for ice mining instead of accessing deeper permanently shadowed craters where larger water deposits might be found. However, the resource availability and extraction viability of



(a) Parallel Hybrid architecture. Dry regolith and icy regolith are processed simultaneously in different sites.



(b) Series Hybrid architecture. Dry regolith from water extraction process is further processed in a PSR.

Figure 1: Hybrid ISRU production plant architectures.

these small PSRs are still highly unknown [41]. Therefore, this scenario has not been considered part of the study.

Although identifying a specific site within the lunar South Pole was out of the scope of this work, previous studies [23, 42, 43] have identified traverse distances of around 0.8-8.5 km between potential human landing system sites, permanently shadowed craters where acceptable water ice deposits might be found, and ridges with prolonged sunlight availability. A preliminary analysis demonstrated that mass and power budgets were not sensitive to changes in the traverse distance. Therefore, an average traverse distance of 5 km between PSRs and PELs is employed in this study as depicted in Fig. 1.

As a baseline case scenario, the ISRU plant is assumed to produce 10 tons of O_2 and 1.25 tons of H_2 per year. This 8:1 ratio corresponds to the stoichiometric mass ratio of water to maximize the use of local resources for various purposes. It is

worth noting that, for hydrolox lunar ascent vehicle propellant, the fuel mixture mass ratio is generally close to 6:1. Some past studies employed this 6:1 ratio or a similar ratio as their required products ratio allowing an excess of oxygen [23, 44].

The integrated hybrid production plant model in this paper includes all the necessary ISRU subsystems, from regolith excavation to cryo-storage of the produced O_2 and H_2 (see Section 4 for a detailed explanation of the models), except for power, thermal control (i.e., radiators), and water purification subsystems. The infrastructure and operations to further utilize these products are not addressed in this work.

Margins are included in the mass budgets following the methodology of the American Institute of Aeronautics and Astronautics Mass Properties Standard [45]. This standard recommends a minimum increase of 30% of the estimated subsystem mass to include a growth margin as well as an additional margin that accounts for uncertain packaging and

Table 1
Global study assumptions.

Required production rate (baseline)	10 t/a of O ₂ and 1.25 t/a of H ₂
PEL/PSR traverse distance	5000 m
Mass margin	30%
Power margin	30%
PEL avg. temperature	200 K
PSR avg. temperature	80 K
Outer space temperature	4 K
Dry regolith density ¹	$\rho_{\text{dry}}(z \text{ in m}) = 1800 - 700 \cdot e^{-z/0.06}$ (in kg/m ³)
Icy regolith density ²	$\rho_{\text{icy}}(\text{wt}\%_{\text{ice}}) = \rho_{\text{dry}} \cdot (1 + \text{wt}\%_{\text{ice}})$ (in kg/m ³)

¹ z is the regolith depth in meters, with $z = 0$ m at the lunar surface. Based on Hayne et al. [46].

² The icy regolith density is calculated assuming that water ice mass fraction (wt%_{ice}) accumulates uniformly within the regolith pores.

structural or neglected components. Similarly, a 30% margin is considered for the power budget.

Table 1 collects the global assumptions considered in this study, including the radiative outer space and average surface temperatures for each site, which are used for the heat loss and radiative heat exchange calculations, and the dry and icy regolith density dependencies on depth and water ice content. Individual assumptions are described for each model in Section 4. Moreover, Section 6 discusses the values of the following uncertain parameters considered in this study: feedstock particle size, silicate and water ice content in the regolith, water extraction efficiency, and ISRU plant operational availability.

3.2. Technology selection

Over the last decades, numerous strategies for extracting oxygen from dry lunar regolith have been proposed in the literature [4, 25, 47]. From these strategies, ilmenite reduction by hydrogen followed by the electrolysis of water and carbon-based reductants (e.g., CO, CH₄, C) has been considered as feasible and viable options [47]. Carbothermal reduction of partially molten regolith, with water electrolysis and CH₄-reforming, the direct electrochemical reduction of molten regolith, the electrolysis in a bath of molten salts, or vacuum thermal decomposition of lunar soils, have also been extensively researched [4].

Carbothermal Reduction (CR) of partially molten regolith is chosen as O₂ extraction technology in this study due to its high yield, as it can reduce most regolith minerals, including the most prevalent silicates. Hydrogen reduction is excluded from further consideration since hydrogen is

mostly limited to reducing iron-bearing minerals such as ilmenite, which are expected to only present in about 0.5 wt.% of the lunar Southern polar highland regolith [48]. As demonstrated by Guerrero-Gonzalez and Zabel [32], the low ilmenite content significantly increases the total hardware mass of the plant, highlighting its ineffectiveness as an oxygen extraction technology in these polar regions.

Moreover, other O₂ extraction technologies, such as electrochemical reduction or vacuum thermal decomposition, do not produce water but oxygen directly from the regolith. Therefore, selecting either of these technologies could lead to larger total system mass and power due to the lack of a shared H₂O electrolysis infrastructure.

The extraction of water (or hydroxyls) can be done by heating lunar icy regolith until volatiles vaporize or desorb, followed by capturing the released gases [4]. Generally, heat can be applied to the icy regolith by electric heating or concentrated sunlight. Note that an alternative approach of using microwave heating also has gathered attention for its potentially higher extraction efficiency[24], which should be further discussed in the future. The process of thermal extraction relies on the low-pressure environment on the Moon for sublimation to occur. By avoiding the liquid phase of water, the produced water vapor can outgas and be captured.

The main two principles of operation include in-situ water extraction through direct surface heating [15, 17, 18] or drill rods [19, 20], and excavation and transportation of icy regolith into an enclosed system followed by subsequent heating. This heating process can be continuous [21] or in batches [22]. Kiewiet et al. [22] traded off in-situ against excavated water extraction methods, with the excavated designs generally scoring significantly better than the in-situ ones. Therefore, in this study, an excavator delivers icy regolith to a water extraction plant, where water is thermally extracted in crucibles.

3.3. Concept of operations

3.3.1. Parallel Hybrid architecture

Six systems are involved in the overall concept of operations of the Parallel Hybrid ISRU production architecture: (1) a dry-regolith mining (excavation and disposal) system, (2) a dry-regolith processing plant, (3) an H₂/O₂ production and storage plant, (4) an icy-regolith mining (excavation and disposal) system, (5) an icy-regolith processing plant, and (6)

a water transportation system between both ISRU plants, as depicted in Fig. 1a.

At the PEL, an excavator delivers dry regolith to the processing plant to extract oxygen. To avoid disturbances, the excavation site is located 100 m away from the ISRU facility [7]. After delivering a fresh regolith batch, the same vehicle is loaded with ISRU-produced tailings and drives first to a disposal site, also located 100 m away, before going back to the excavation site. The dry-regolith excavator recharges at the dry-regolith processing plant.

At the PSR, a similar scenario is defined. Another excavator delivers icy regolith to the icy-regolith processing plant, collects dry processed regolith, and dumps it at a disposal site before going back to the icy-regolith excavation site. The three locations are also positioned 100 m away from each other. The number of excavators for the dry- and icy-regolith is calculated based on the processing times, travel times, and regolith throughputs needed. The icy-regolith excavator only recharges at the icy-regolith processing plant without leaving the PSR.

A similar mobile water transportation solution to the one discussed by Kleinhenz and Paz [23] is chosen to allow for a fair comparison between different system architectures. A tanker remains at the icy-regolith processing plant to directly capture water into its tank, while others deliver H₂O to the H₂/O₂ production plant and come back to the PSR. This approach saves hardware mass since water vapor is allowed to freeze directly inside the tank, avoiding the need for additional cold traps. Moreover, due to the low PSR temperatures, no power is required to maintain the state of water ice. Once the tanker leaves the PSR, water starts to thaw due to solar radiation. The water tankers recharge at the H₂/O₂ production and icy-regolith processing plants. The total number of the water tankers is selected from a range of two to 10 to minimize the total landed mass of the entire system. This number affects travel times, tanker capacity, water throughputs, and processing times needed.

Liquid water delivered to the H₂/O₂ production plant is subsequently electrolyzed into hydrogen and oxygen. Together with the oxygen extracted from dry regolith, they are liquefied and cryogenically stored.

3.3.2. Series Hybrid architecture

The Series Hybrid architecture (Fig. 1b) involves placing both the dry- and icy-regolith processing plants within the PSR to further process dry regolith after water extraction

to obtain oxygen. Water extracted from icy regolith and generated through carbothermal reduction is transported to a PEL for electrolysis, liquefaction and storage, requiring the same water tanker system as the Parallel Hybrid architecture.

By processing excavated icy regolith utilizing multiple technologies, this architecture can potentially achieve the highest oxygen yield per unit mass of excavated regolith, leading to slower excavation rate. However, significant operational and technological challenges also arise in this architecture. Colder surface temperatures would negatively affect high-temperature ISRU processes, increasing energy consumption where no direct sunlight as a power source is available.

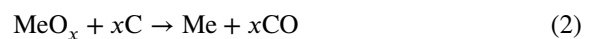
4. Lunar ISRU hybrid plant modeling

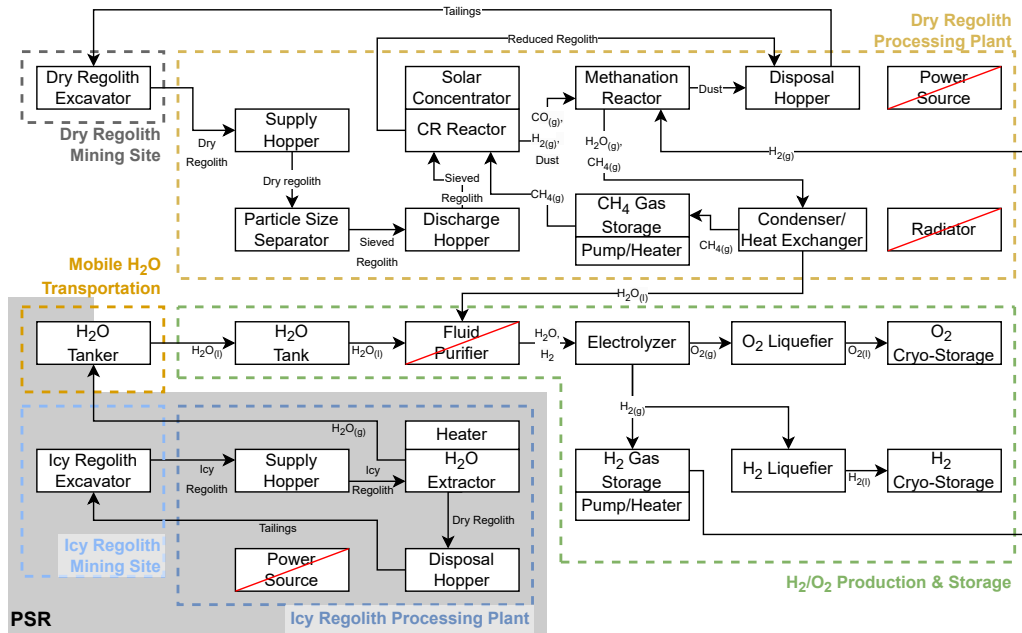
Fig. 2 shows the system architectures selected for this study. For each subsystem, a technology is modeled using ISRUlib. ISRUlib is an open-source component- and system-level library of ISRU models developed by the Technical University of Munich to carry out high-level technological trade-offs and preliminary architectural definitions [49]. To estimate the mass and power of the hybrid architectures proposed in this paper, parametric sizing models for carbothermal reduction and water extraction subsystems are newly developed and added to ISRUlib. The models estimate mass and power budgets, as well as the performance of different technologies, based on analytical parametric calculations, extrapolated experimental results, surrogate models from numerical simulations, and already existing ISRU hardware.

4.1. Carbothermal reduction of dry regolith

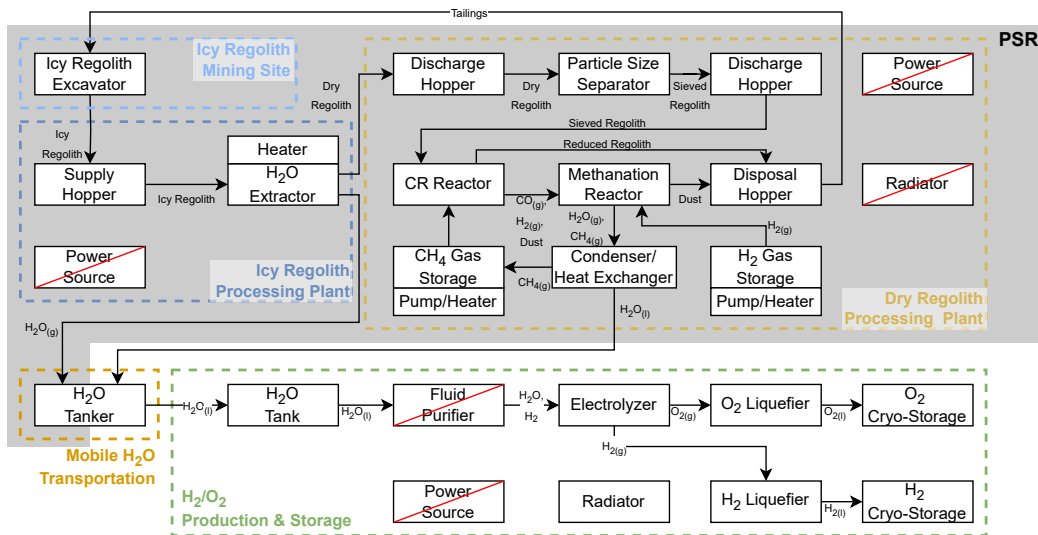
Carbothermal reduction (CR) is the process of reducing partially molten (often metal) oxides using carbon in a form, such as methane, as a reducing agent. This process generates carbon monoxide, which can be further processed to reform CH₄ and produce oxygen via water electrolysis. Historically, the CR process followed by methanation has been researched [7–9] and demonstrated extensively to extract oxygen from lunar regolith simulants [10, 11].

The chemical process can be generally expressed as:





(a) Parallel Hybrid architecture.



(b) Series Hybrid architecture.

Figure 2: System architecture of the hybrid ISRU production plants. Mass flows across subsystems are shown. The diagram blocks crossed out in red are not modeled.

where MeO_x and Me represent a general metal oxide and metal, respectively. CR can process the silicate minerals and iron-bearing minerals in lunar regolith [8]. Gustafson et al. [50] report that because of the widespread distribution of suitable metal oxides for CR on the lunar surface, mineral enrichment is not likely required for CR. However, it is still necessary to classify as-mined regolith by size to improve

the reaction efficiency [51]. In this paper, it is assumed that the size-sorting beneficiation (see Section 4.3.2) is applied before the CR process.

Silica (SiO_2) is the most abundant metal oxide in highland regolith, and is the focus of this work. While CR is capable of reducing various metal oxides at different temperatures,

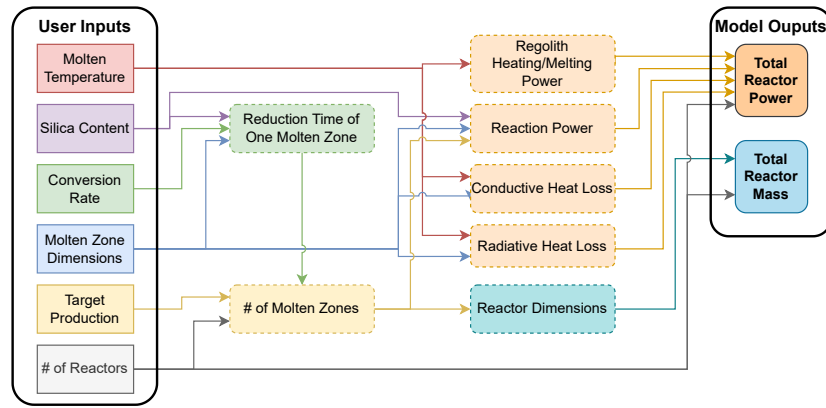


Figure 3: High-level schematic of a parametric sizing CR reactor model.

capturing this capability in the model adds considerable complexity with diminishing returns on fidelity.

The reaction of silica with methane has been extensively modeled by Balasubramaniam et al. [52]. The reaction



occurs at 1250-2000 °C [53]. To achieve such high temperatures, Balasubramaniam et al. [52] and Linne et al. [7] proposed the use of solar thermal energy to melt a concentrated area of regolith. These studies also suggested to use regolith as a thermal insulator to protect reactor walls from molten regolith. The use of concentrated solar thermal energy has been experimentally simulated using lasers to demonstrate the CR process of lunar regolith simulants in vacuum conditions [10].

Figure 3 depicts a high-level schematic of the parametric sizing model used for CR reactor mass and power estimations. From silica content in the regolith, conversion rate, and dimensions of a molten regolith zone, the reaction time of one molten zone can be calculated using the model developed by Balasubramaniam et al. [52]. The estimated reaction time is used to calculate the minimum number of molten zones required to meet the target production rate. The number of molten zones can affect the dimensions of the reactor design, which affects the total mass of the reactor (see Fig. 4 for the design of the reactor). The main material of the reactor and its minimum allowable wall thickness is set to Inconel and 3.0 mm, respectively.

The total power required from the solar concentrator can be divided into four: power for heating and melting the regolith, for carrying out the reaction, and the conductive

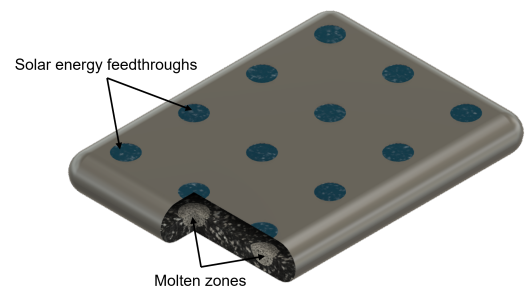


Figure 4: CR reactor design. The number of molten areas is the same as the number of solar energy feedthroughs, which affects the dimensions of the reactor.

and radiative heat losses to the environment. The heating power can be derived from the heat capacity of the regolith, which is modeled in the literature [54, 55]. The latent heat of lunar highland regolith is calculated as 478.6 kJ/kg by Schreiner et al. [56]. The enthalpy of the reactions described by Equations 1 and 4 are reportedly 75.6 kJ/mol and 689.8 kJ/mol, respectively [57]. The conductive heat loss can be calculated from the geometry of the molten zone and the reactor, and the thermal conductivity of lunar regolith. Cremers and Hsia [58] reported the thermal conductivity of Apollo 16 highland regolith as $1.0 - 1.5 \times 10^{-3} \text{ W}/(\text{m} \cdot \text{K})$ at around 400 K. Due to this extremely low thermal conductivity of lunar regolith, the conductive heat loss can be practically ignored. The radiative heat loss can be calculated from the molten zone geometry and its temperature and the environment temperature. Following the assumptions made in [57], we use 0.7 as the emissivity of molten regolith, and we assumed that there is an insulation cover on each molten zone with a small hole on it. Due to these insulation covers, the radiation loss can be limited to 6.25% of the case without

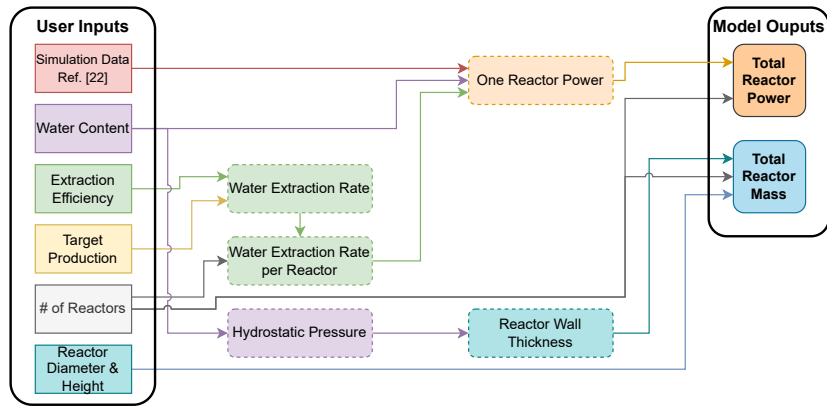


Figure 5: High-level schematic of a parametric sizing WE reactor model.

the covers. With these assumptions, the heat loss from one molten zone can be calculated as about 26.6 W.

The mass of the methanation chamber is modeled based on the work of Schrenk [59]. In this model, the mass of a Sabatier chamber is scaled based on a mass of those demonstrated in literature such as [60]. Following Ref. [59], the specific mass used for the methanation subsystem is 17.9 kg per 1.0 kg/h of water produced.

4.2. Water extraction from icy regolith

In the proposed architecture, water from icy regolith is thermally extracted in crucible water extractors [22, 61] in a PSR. The performance of these crucible water extractors is modeled following the work of Kiewiet et al. [22]. Each extractor has resistive heaters providing the required heating power. It is assumed that the entire extraction process, from icy-regolith excavation to water storage, has a 75% mass recovery efficiency to account for line losses and losses occurring during excavation or vapor capturing. This value is in agreement with the assumptions made by Kleinhenz and Paz [23].

Kiewiet et al. [22] have optimized the heating time of a reactor with different input power and different water ice content to maximize the water yield using the COMSOL Multiphysics® software. In their study, the water content of 1, 5, and 15 weight % (wt%), and the input power of 500, 1500, and 2500 W were selected to see their effect on water extraction rate and energy efficiency.

Figure 5 depicts a schematic of water extractors' mass and power estimation developed for this paper. From the extraction efficiency and the target oxygen and hydrogen production rate, the target water extraction rate can be

calculated. From the relationship between the input power to an extractor, the average water ice content in excavated regolith, and the water extraction rate, mentioned above, the model can estimate the required power. Note that the relationship is fit to a quadratic equation from the data points from [22], and the maximum allowable power input per reactor is set to 2500 W to avoid extrapolation on the higher power side. When the input power requirement exceeds 2500 W, the number of reactors is modified iteratively.

The mass of the reactor is estimated from the crucible reactor design with a diameter of 0.46 m and a height of 1.0 m [22]. Ignoring other volatile gases, the required wall thickness is calculated from hydrostatic pressure based on the water content with a minimum thickness of 3.0 mm and Inconel is selected as reactor material.

4.3. Supporting subsystems

Besides the principal oxygen and water extraction processes, the required supporting subsystems, including shared infrastructure, are also modeled to provide a holistic end-to-end representation of the entire ISRU production plants. This subsection briefly summarizes the excavation, beneficiation and water transportation subsystems. For the shared subsystems, see Section. 4.4.

4.3.1. Excavation and handling subsystem

The excavator models are based on NASA's Regolith Advanced Surface Systems Operations Robot (RASSOR) 2.0 [62]. RASSOR 2.0 includes two sets of two bucket drums that produce opposing digging forces, causing a net-zero horizontal reaction force and enabling its operation under reduced lunar gravity. To adapt the models to the conditions

of each excavation site, the regolith density is modified according to depth and water ice content.

Both excavators deliver regolith to hoppers sized to accommodate three batches of the H₂O extractor and CR reactor, respectively, to account for buffer storage due to operational mismatches. The discharge and disposal hoppers of the dry-regolith processing plant are made of Inconel to withstand the carbothermal reduction temperature. Since both supply hoppers and the disposal hopper of the icy-regolith processing plant have to withstand lower operating temperatures, aluminum is selected as a structural material in this case.

4.3.2. Beneficiation subsystem

A particle size separator is included to remove the coarse regolith fraction. Although the particle size effect on the carbothermal reduction of lunar regolith is not well-researched, Samouhos et al. [51] claim that the smaller particle size leads to higher efficiency in the reduction by increasing the relative surface area between regolith and carbon. Haas and Khalafalla [63] also reported a decreasing efficiency of carbothermal reduction around the silica particle size of 0.13 mm. Without further information on particle size effects on carbothermal reduction of lunar regolith, this paper assumes that the particle size separator removes particles with a diameter larger than 0.15 mm. The particle size separator is based on the model by Linne et al. [7], where a trough covered by a size-sorting grate dumps regolith from a hopper to an auger conveyor that transports the granular material to the next subsystem.

4.3.3. Water transportation

The model developed by Kleinhenz and Paz [23] is considered for the water tankers discussed in Section 3.3. The tankers are composed of a mobility platform and a payload, which includes a water tank, a battery, and a communication and navigation unit. The mobility platform mass is based on a payload ratio (payload mass/mobility platform mass) of 1.5, similar to RASSOR 2.0. The aluminum tank is modeled based on its water capacity, including a 50% ullage. The battery energy density is 140 Wh/kg, allowing for a maximum 80% discharge. These same battery properties are used for the RASSOR 2.0 excavators. The charging stations at the propellant production and H₂O extraction plants can provide enough power to allow for a 5-hour excavator and a 10-hour tanker recharge time.

The tankers deliver water to a fixed aluminum tank at the H₂/O₂ production plant, which is 3 times larger than the total tankers' water tank volume to account for operational mismatches. The water tank mass also includes a Commercial-Off-The-Shelf (COTS) pump, which is modeled based on those for space applications by Micropump, Inc. [26, 64]

4.4. Shared infrastructure

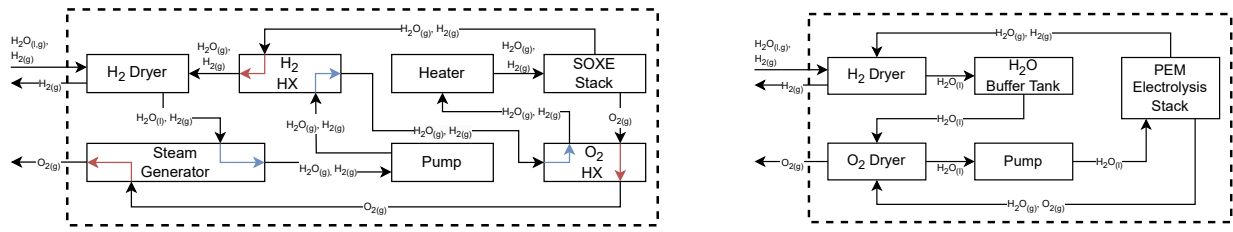
Most of the shared infrastructure between the oxygen and hydrogen coproduction from lunar icy and dry regolith is shown in green in Fig. 2. This shared infrastructure includes the water tank and electrolyzer, the H₂ and O₂ liquefaction and cryostorage subsystems, and high-pressure tanks to supply gas for the carbothermal reduction, accounting for buffer storage due to operational mismatches. A COTS pump is included before the pressurized vessels to store H₂ and CH₄ at 300 bar, and 200 bar, respectively [65], and average PEL temperature. It must be noted that the energy required to cool down the exhaust gas stream before the electrolysis is partially recuperated and used to preheat the intake methane stream. Therefore, an additional Condensing Heat Exchanger (CHX) is included between the pressurized vessel and the reactor to further increase the gas temperature to the operating temperature.

It must be noted that no fluid purifier is considered in this study. The criteria for designing such a subsystem are largely undefined since lunar water contaminants are yet to be fully characterized [66].

4.4.1. Electrolysis subsystem

Different water electrolysis technologies, such as high-temperature Solid Oxide Electrolysis (SOXE) [67], Proton Exchange Membrane (PEM) electrolysis [68], or alkaline electrolysis [69], have already been discussed in the context of space exploration [70]. In this study, the two most commonly researched electrolysis architectures, SOXE and PEM (Fig. 6), are evaluated regarding their subsystem mass and required power.

Table 2 lists the mass and power consumption estimated for both systems sized to generate 10 t of oxygen and 1.25 t of hydrogen per lunar year. The mass and power in this table are summations of all components shown in Fig. 6. As can be seen in Table 2, the mass of the PEM electrolysis subsystem can be significantly lighter, whereas the SOXE electrolysis requires less power. As further discussed in Section 5.1, this difference in mass between these two systems can be trivial compared to the entire system mass. Conversely, the electrolysis subsystem



(a) High-temperature Solid Oxide Electrolysis (SOXE). Inside the steam generator and Heat Exchangers (HXs), heat is transferred from the hot (red) to the cold (blue) fluid streams.

(b) Proton Exchange Membrane (PEM) electrolysis.

Figure 6: Electrolysis subsystem (Electrolyzer) architectures. Mass flows across components are shown.

Table 2

Mass and power comparison of water electrolysis technologies. Sized for 10 t of oxygen per lunar year.

	Mass (kg)	Power (kW)
PEM	9.1	23.00
SOXE	100.6	7.18

is one of the main power drivers, and the difference between these two technologies (i.e., ~ 16 kW) can have a significant impact. Therefore, this paper employed the SOXE subsystem for further analysis.

4.4.2. Gas liquefaction and storage subsystem

Johnson et al. [71] compared several oxygen liquefaction methods for use on the Martian surface. From their analysis, the tube-on-tank cycle was adopted for both hydrogen and oxygen liquefaction in this study due to its performance and simple adaptation to the lunar environment. The system consists of a tank equipped with small tubes mounted around its external wall. The working fluid circulates through the tubes and is cooled by a series of cryocoolers. The cryogenic tanks are sized in aluminum to accommodate the entire yearly gas production. No additional power is included for storage maintenance because the system is a zero boil-off design.

5. Mass, power, and sizing results

In this section, the mass and power budgets of the hybrid ISRU plant are compared with more conventional plant architectures. The budgets were estimated using the model described in Section 4. The landed mass and required power of each architecture are compared following the baseline case (Section 5.1) and sensitivity analyses are conducted in Section 5.2. The developed model is further compared with past studies in Appendix A.

5.1. Comparison of Resource Extraction Architecture

To compare all architectures, each plant is designed to produce the same LOX amount. Since the hydrogen generated from the CR process is recycled for the methanation process (Equation 3), additional LH₂ and its storage tank are assumed to be brought from Earth to compensate for the lack of produced hydrogen. Furthermore, even though both methane and hydrogen are recycled in the CR process, their recycling rate is unlikely to be 100%. Lavagna et al. [72] reported a recycling rate of 91% from their experiments. In this paper, we use this value of 91% as a baseline recycle rate assuming additional gaseous methane and hydrogen are brought to the Moon to compensate for this reactant loss. Due to the additional methane and hydrogen from Earth, the comparable landed masses on the Moon of the CR architecture, and all hybrid architectures depend on the operational period. Table 3 lists the estimated mass and power of each subsystem of each plant architecture scaled to produce 10 t of LOX per lunar year with 1.25 t of LH₂ either produced or brought to the plant additionally. The Parallel Hybrid architecture on this table is designed to produce 5.0 t of LOX from water generated from the methanation, and the rest from the water from the PSR.

Table 3: Mass and power estimation of each architecture. Sized for 10 t of oxygen and 1.25 t of hydrogen per lunar one year. The operational period is set to one year.

Element	Mass [kg]*1			Power [W]*1				
	CR	WE	Parallel*2	Series	CR	WE	Parallel*2	Series
Dry regolith mining								
Excavator	111	-	111	-	633	-	633	-
Dry regolith processing								
CR reactor	299	-	116	299	66,010	-	33,005	50,604
Methanation reactor	54	-	27	42	-	-	-	-
Other dry regolith processing subsystems*3	33	-	32	29	2	-	1	1
Icy regolith mining								
Excavator	-	111	111	111	-	633	633	633
Icy regolith processing								
H ₂ O extractor	-	461	230	115	-	25,918	12,959	5,593
Other H ₂ O extraction subsystems*4	-	221	99	194	-	-	-	-
Mobile H₂O transportation								
H ₂ O tanker	-	2,557	1,014	2,557	-	1,769	673	1,769
H₂/O₂ production and storage								
SOXE electrolysis subsystem	101	101	101	101	7,183	7,183	7,183	7,183
Liquefaction subsystem	192	1,870	1,039	680	5,616	28,093	16,855	12,038
Storage and recycle subsystems	348	551	518	450	71	0	69	70
Additional materials from Earth								
Additional H ₂ and tankssubsystems*5	2,161	-	1,101	1,664	-	-	-	-
Additional CH ₄ and tankssubsystems*6	966	-	491	746	-	-	-	-
Total	4,265	5,872	5,051	6,988	79,515	63,596	72,010	77,892

* 1: All values include 30% growth [45] except for additional H₂ mass.

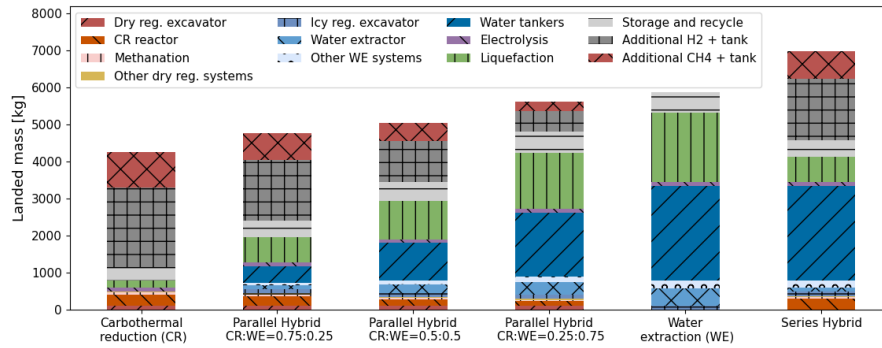
* 2: 5 t of LOX is generated from CR and the rest 5 t from WE (1:1 ratio).

* 3: Supply and discharge hoppers, and particle size separators.

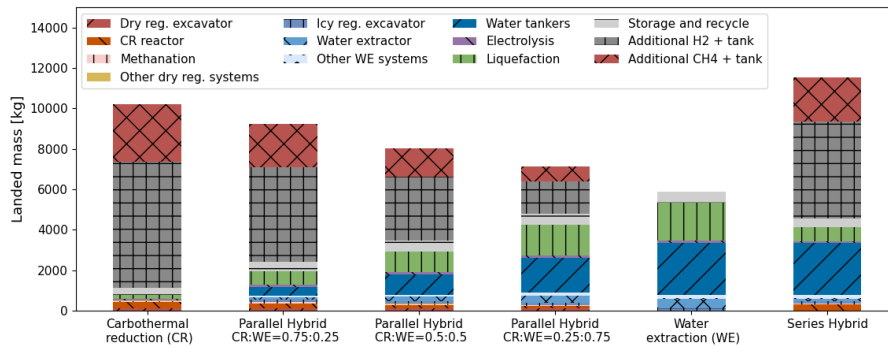
* 4: Supply and discharge hoppers.

* 5: Additional H₂ for reactant loss (91% recycling efficiency) and product compensation.

* 6: 91% recycling efficiency.



(a) One-year operation.



(b) Three-years operation.

Figure 7: Mass comparison.

Figures 7 and 8 are bar charts of mass and power breakdown. In addition to the four architectures in Table 3, the Parallel Hybrid architectures with different hybrid ratios are added. The landed mass of the CR architecture turned out to be the lightest compared to the others for one year of operation (Fig. 7a). As the operational period becomes longer, the additional hydrogen and methane from Earth become heavier, making the WE architecture the lightest (Fig. 7b). The main mass drivers other than additional methane and hydrogen are the water tankers and the liquefaction subsystem. Since liquefying hydrogen requires heavy cryocoolers (see, e.g., Deserranno et al. [73]), the liquefaction subsystem of the CR architecture becomes the lightest. The Series Hybrid architecture turns out to be the heaviest in both analyzed operational periods. This is because the Series Hybrid architecture largely depends on oxygen from CR rather than WE, requiring additional hydrogen and methane from Earth. Furthermore, since all water is produced in the PSR, this architecture requires the same amount of water tankers as the WE dedicated plant, which is another major mass driver.

Figure 8 is the bar chart of the power breakdown. The main power drivers are the CR reactor, the water extractor, the electrolysis subsystem, and the liquefaction subsystem. As can be seen, the water extractor itself requires significantly less power than the CR reactor. However, due to the liquefaction of hydrogen, the total difference in power consumption between the CR and WE architectures is about 16 kW.

5.2. Sensitivity Analyses

The effect of the target production rate on the comparable mass and the power consumption are summarized in Figs. 9, and 10. As can be seen, there are near-linear trends for both mass and power against the production rate. Among the analyzed range, 1 – 20 tons of oxygen per year (Fig. 9a), the Series Hybrid architecture is always the heaviest. While the CR architecture can be the lightest regardless of the target production for one year of operation (Fig. 9a), for three years of operation (Fig. 9b), the advantage of the WE architecture becomes clearer due to the extra methane and hydrogen required for the other architectures. When comparing the power consumption Fig. 10), the WE plant appeared to be the

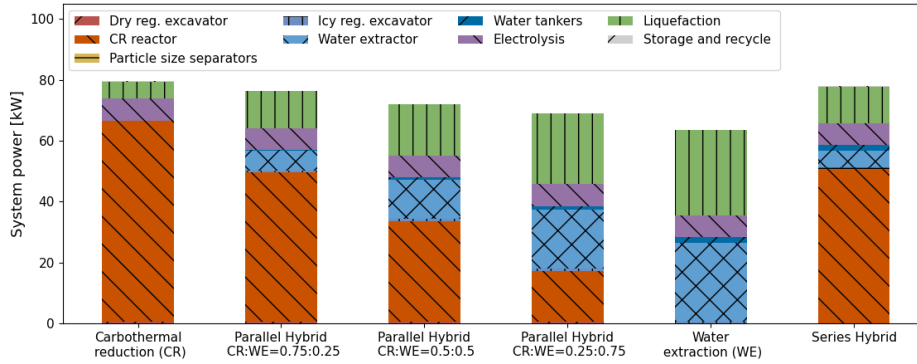


Figure 8: Power comparison.

least power-consuming while the CR or the Series Hybrid plant requires the most power.

Figure 11 shows the system mass dependence on the CR reactant, i.e., CH_4 and H_2 , recycle rate. As can be seen in this figure, there is a linear relationship between the recycle rate and the landed mass. For one year of operation (Fig. 11a), the CR can be the lightest architecture. For a higher recycling rate, the difference between the WE and the Series Hybrid architecture can be almost negligible. When the operational period is three years (Fig. 11b), the WE can be the lightest regardless of the CR reactant recycle rate.

Water ice content in the excavated regolith in a PSR also affects the comparable landed mass and the power consumption of the WE and the hybrid plants significantly (Figs. 12 and 13). Generally, as water content increases, both the landed mass and power consumption decreases. This trend affects both the lightest plant architecture and the least power-consuming plant architecture. As can be seen in Fig. 12a, the water content has the largest impact on the mass of the WE architecture for one year operation. However, for three years' operation, the landed mass of the Series Hybrid architecture becomes significantly lighter as the water content becomes larger. This is because as the water content increases, the Series Hybrid architecture depends more on the WE from the icy regolith rather than the CR of the dry regolith, making the system mass for dry regolith processing smaller. Since the CR architecture can be a lot heavier than the WE architecture for the three years of operation, the Series Hybrid architecture can be lighter by depending less on the CR architecture. The water content in the PSR is further considered for uncertainty analyses (Section 6.1.3).

Table 4

Monte Carlo parameters for uncertainty consideration.

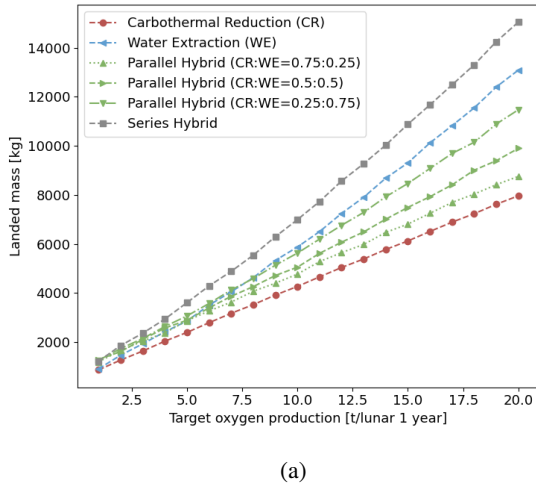
Variable	Distribution (μ, σ^2)
Particle size mass fraction (wt%)	$\mathcal{N}(62.6, 8.3^2)$
Silica content (wt%)	$\mathcal{N}(45.2, 0.93^2)$
Water ice content (wt%)	Nominal: $\text{Lognormal}(\ln(4), 0.3^2)$ Best: $\mathcal{N}(30, 2^2)$
Water yield (-)	$\mathcal{N}(0.75, 0.05^2)$
Operational availability (days/year)	$\mathcal{N}(200, 10^2)$

6. Uncertainty in lunar ISRU

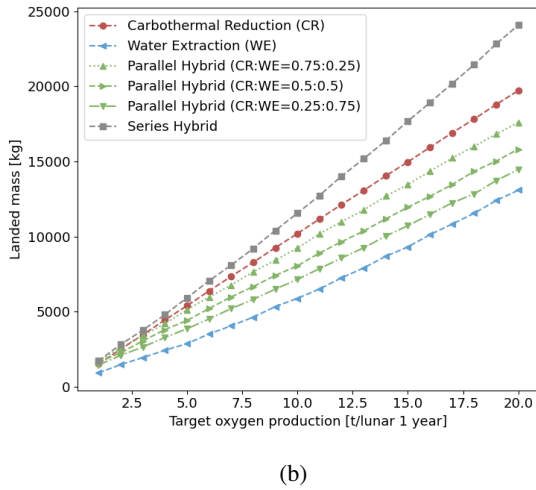
6.1. Uncertain parameters

As Cilliers et al. [31] stated, the effect of resource uncertainty on the performance of lunar ISRU plants has not been explored enough. In Ref. [30], the impact of uncertain parameters, such as resource content and operational availability, is assessed for the hydrogen reduction process on the Moon. The results indicated the risk of oversimplification by ignoring these uncertainties.

To assess the benefits and drawbacks of each ISRU plant architecture compared in Section 5, this paper further analyzes the effects of uncertainties on the performance of the plant. Inspired by Ref. [30], Monte Carlo simulations of 5000 scenarios with different values for parameters related to the lunar environment and ISRU operations is utilized to reveal the performance of each ISRU architecture under various conditions. Table 4 summarizes the Monte Carlo parameters assumed in this study.



(a)



(b)

Figure 9: System mass as a function of target production rate. The CR Reactant recycle rate is set as 91%.

6.1.1. Particle size distribution of lunar highlands regolith

After excavation, the particle size separator removes the coarse regolith fraction (Fig. 2). In this work, to improve the conversion time of the carbothermal reduction, it is assumed that particles larger than particles larger than 150 μm are removed as mentioned in Sec. 4.3.2. A further assumption is that the lunar surface in the southern polar region is mainly covered by highlands regolith similar to Apollo 16 samples [74, 75]. Figure 14 shows the particle size distributions of 75 Apollo 16 samples reported by [76]. From these distributions, Fig. 15 is generated to depict the distribution of the mass fraction of the excavated regolith between 90 and 1000 μm . As can be observed in Fig. 15, the mass fraction is normally distributed with a mean value of 62.6 wt% and a standard

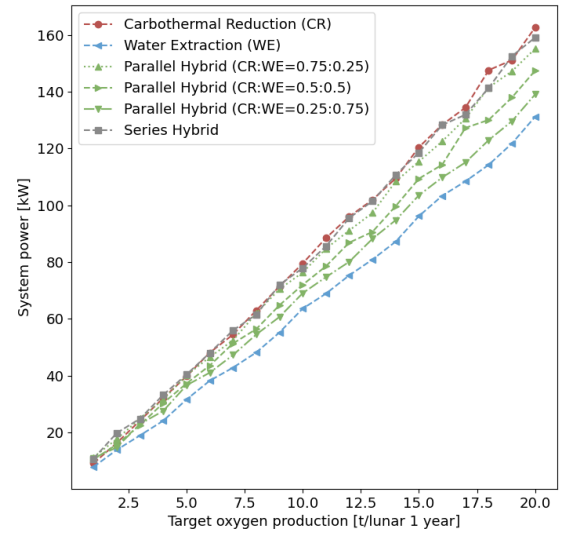


Figure 10: System power as a function of target production rate.

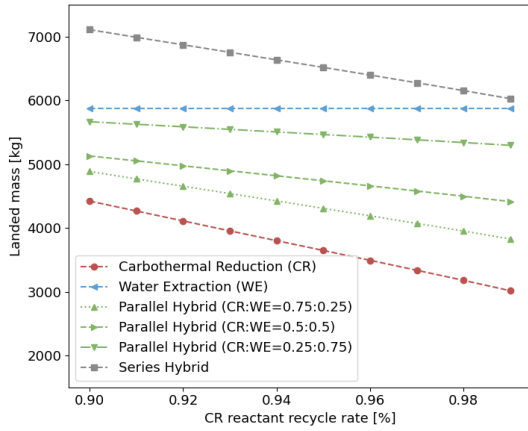
deviation of 8.3 wt%, i.e., $\mathcal{N}(62.6, 8.3^2)$. Therefore, the mass fraction of excavated regolith in the southern polar region is assumed to follow this distribution.

6.1.2. Silica content in lunar highlands regolith

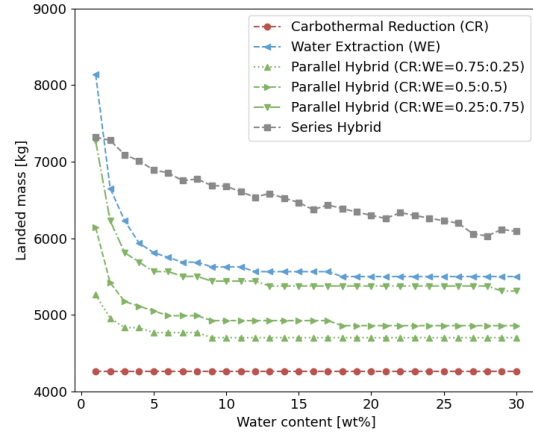
As reported in [77], silica is the most dominant metal oxide in lunar highlands regolith. The Apollo 16 sample 60501 contains 45.24 wt% of silica with a standard deviation of 0.93 wt%. Without further information on the silica content of the lunar southern polar regolith, we also assumed $\mathcal{N}(45.2, 0.93^2)$ as a distribution of the silica content.

6.1.3. Water ice content in the lunar south polar region

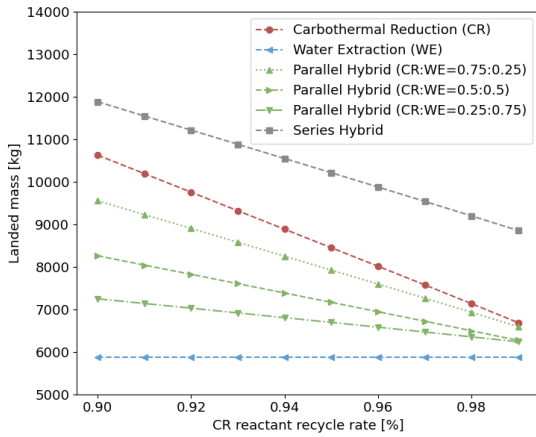
Compared to the silica concentration, information regarding water ice content in the southern polar region of the Moon is significantly more limited. A great number of past studies have tried to estimate the icy water content in PSRs. For instance, Colaprete et al. [36] analyzed Lunar Crater Observation and Sensing Satellite's ejecta plume and concluded that the water ice content in the impact site (Cabeus crater) was 5.6 ± 2.9 wt%. The authors also noted that icy water might exist heterogeneously. Hayne et al. [37] supported this heterogeneity showing some cold traps, where water ice can be thermally stable, do not have exposed water ice. This also aligns with the finding of only 3.5% of PSRs probably having surface ice by Li et al. [38]. From UV albedo values, Hayne et al. [37] concluded that 0.1–2.0 wt% of water



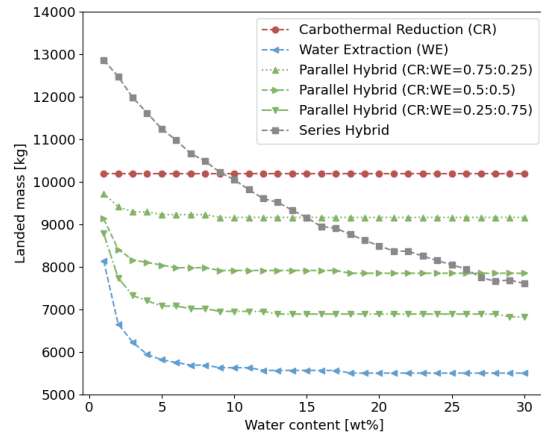
(a) One-year operation.



(a) One year operation.



(b) Three-years operation.



(b) Three years operation.

Figure 11: System mass as a function of the CR reactant recycle rate. Target production mass is set to 10.0 t of LOX and 1.25 t of LH₂.

Figure 12: System mass as a function of water ice content in regolith.

ice might be exposed in some PSRs if the ice is intimately mixed with dry regolith, whereas 1-10% of surface area would be icy if this is pure and patchy.

More recently, using the data from the Moon Mineralogy Mapper, Li et al. [38] estimated the water content in PSRs by detecting near-infrared absorption features of water ice in reflectance spectra. This study revealed that ice-bearing pixels (280 m × 280 m) may contain around 30 wt% of ice intimately mixed with regolith or 20 vol% if pure and patchy ice exists. This is a good agreement with Zuber et al. [78], who concluded that 20% superficial thin (~1 μm) ice may exist in the Shackleton crater. As Cannon and Britt [79] argued, estimations made by Hayne et al. [37] and Li et al. [38] correspond to only surface ice (micrometers to millimeters

depth), whereas the value measured from the Lunar Crater Observation and Sensing Satellite impact might be subsurface data (tenths of centimeters depth).

These past studies indicate significant heterogeneity of water ice in the southern polar region might be expected. With all the information available to this date, it is hard to conclude the water content in excavated icy-regolith. Therefore, this work tests two different scenarios: a nominal and a best-case scenario. In the nominal scenario, the large ice content reported by [38] exists only on the surface, and the actual ice content in the excavated regolith is smaller than that, which aligns with Cannon and Britt [79]. For this scenario, to avoid negative values, a log-normal distribution with a median value of 4 wt% and a variance of 0.3 wt%² is considered

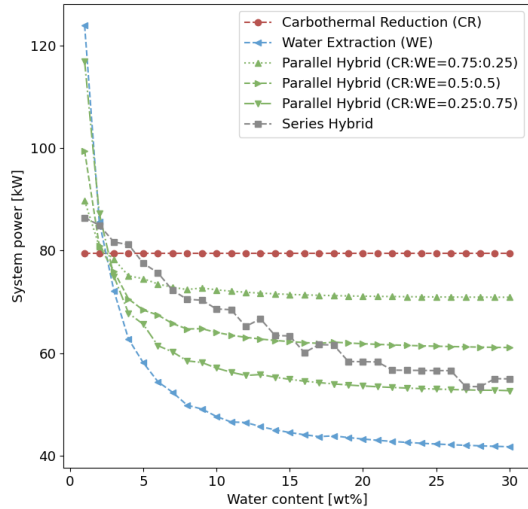


Figure 13: System power as a function of water ice content in regolith.

as the distribution of the ice content. We also test the other scenario where there indeed is more ice in the excavated regolith as reported by [38] within a reachable area from the PEL site. For this scenario, $\mathcal{N}(30, 2^2)$ [wt%] is employed. See Fig. 16 for employed distributions as well as some reported values in past studies.

6.1.4. Water yield

The water yield efficiency of the water extraction technology is another uncertain parameter. Kleinhenz and Paz assumed 75% efficiency [23]. Cole et al. reported $67 \pm 5\%$ of water extraction in 25 minutes of heating from highland regolith simulant [24]. From these studies, this paper assumed 75% mean efficiency with 5% of variance.

6.1.5. Operational availability

Although this work does not prescribe a detailed power system, operational uncertainty related to the power source should be considered. Assuming solar power, operational availability depends on how much sunlight the plant can receive. Mazarico et al. [39] simulated the sunlight availability of many PELs in both northern and southern polar regions (see supplementary tables 2a and 2b from Ref. [39]). According to their simulation, the best location near the ridge of the Shackleton crater can get about 202 days of continuous sunlight which aligns with the assumption made by Linne et al. [7] Therefore, a normal distribution $\mathcal{N}(200, 8^2)$ [days per lunar year] is assumed in this paper.

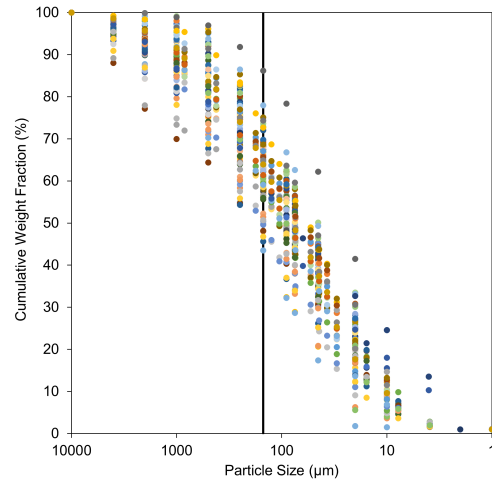


Figure 14: Particle size distributions of 75 Apollo 16 samples obtained from [76]. The black vertical line represents 150 μm .

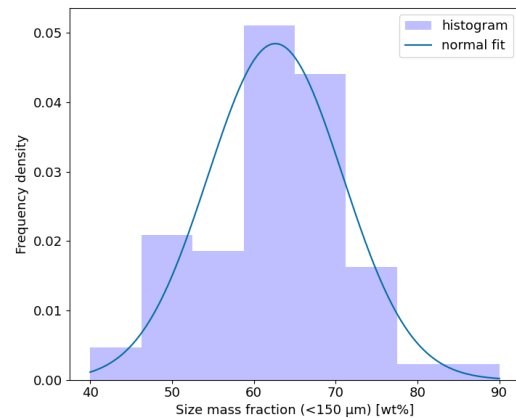


Figure 15: Distribution of mass fraction of 75 Apollo 16 samples with a particle size smaller than 150 μm .

6.2. Lunar ISRU performance under uncertainty

Using the varying parameters listed in Table 4, we run Monte Carlo simulations for 5000 scenarios. Figure 17 depicts the regolith excavation rate of each architecture. As can be seen in this figure, the CR and the Series Hybrid architectures require much smaller excavation rate than the WE and the Parallel Hybrid architectures. This is due to the high oxygen yield of the CR technology compared to the WE technology. The Series Hybrid architecture can potentially achieve a higher yield than the CR architecture by extracting oxygen from both regolith and water ice. However, due to the distance between a PEL and PSR, hydrogen generated in the PEL is not recycled to Reaction 3 in this architecture. This limitation leads to the yield of this Series Hybrid architecture being lower than the CR architecture. The uncertainty in the

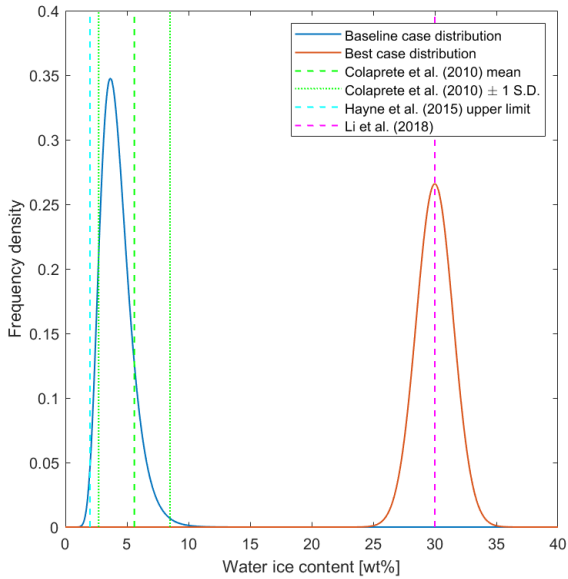


Figure 16: Water ice content.

water ice content makes the required regolith excavation rates for the WE and the Parallel Hybrid architectures unclear. For instance, for the WE architecture, 82 kg/h of regolith excavation is required to produce 10 t of liquid oxygen and 1.25 t of liquid hydrogen with a 50% confidence. However, to achieve a 95% confidence, the required excavation rate becomes 130 kg/h. According to [62], RASSOR is designed to excavate at least 2.7 t of regolith per day (112.5 kg/h). Therefore, depending on the condition, the WE architecture has a risk of not meeting the excavation mass target unless a redundant excavator is considered.

Figure 18 shows the histograms of power consumption of each architecture with varying parameters. As can be seen, the average required power of the hybrid architectures and the CR architecture does not show significant differences. Although the average power consumption of the WE architecture is lower than the other architectures, due to the larger uncertainty in the water ice content, the histogram of the WE architecture shows the widest variety in its power consumption. The non-normality observed in this figure is due to the non-continuity of some design parameters. For instance, the number of molten zones for the CR process and the number of cryocoolers to liquefy oxygen and hydrogen must be integers, making several peaks in the histograms.

Figures 19 and 20 are the results of the Monte Carlo simulations with the best-case water content (i.e., $\mathcal{N}(30)$,

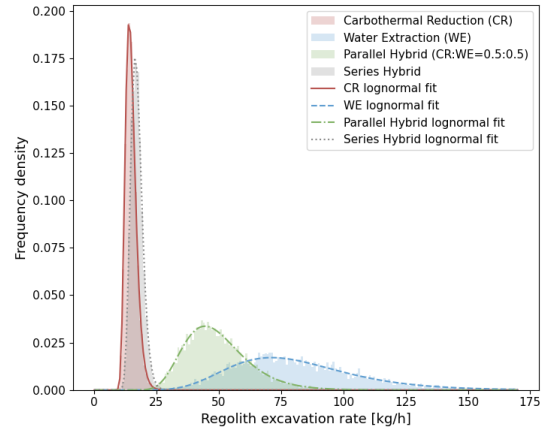


Figure 17: Excavation rate to meet target production, 10 t of LOX and 1.25 t of LH₂.

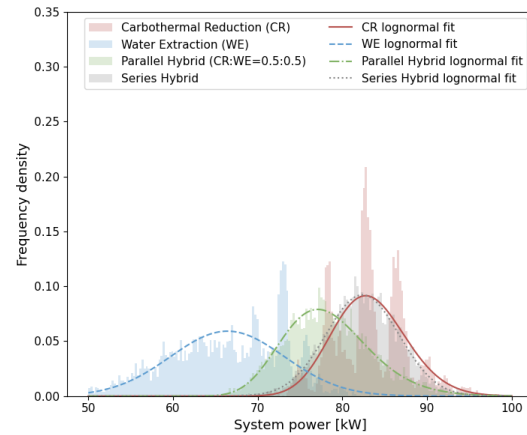


Figure 18: Power consumption to produce 10 t of LOX and 1.25 t of LH₂.

2²). With this abundance of water ice in the lunar southern pole, the the Series Hybrid architecture outperforms the other architectures in terms of the regolith excavation rate (Fig. 19). For power consumption (Fig. 20), the WE plant is expected to require the least. The similar non-normality seen in Fig. 18 is observable in Fig. 20, too.

Finally, the required comparable mass including the additional hydrogen and methane for one year's operation are summarized in Fig. 21. For both water ice content distributions, the CR plant mass variance is significantly smaller than the others. In terms of the expected system mass, the lightest architecture is the CR while the heaviest is the Series Hybrid architecture. For the best-case water ice content (Fig. 21b), the heavier ends of the required landed mass distributions of the WE and the Series Hybrid architectures

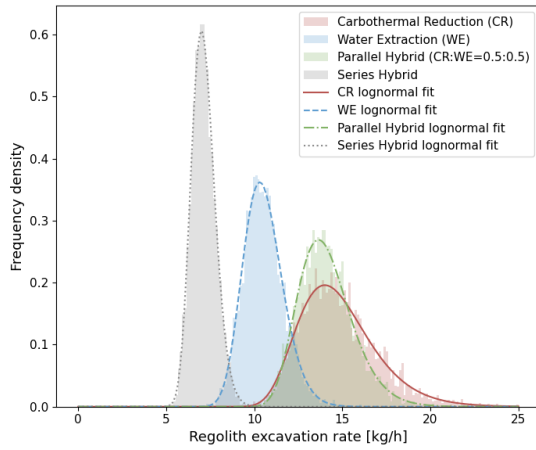
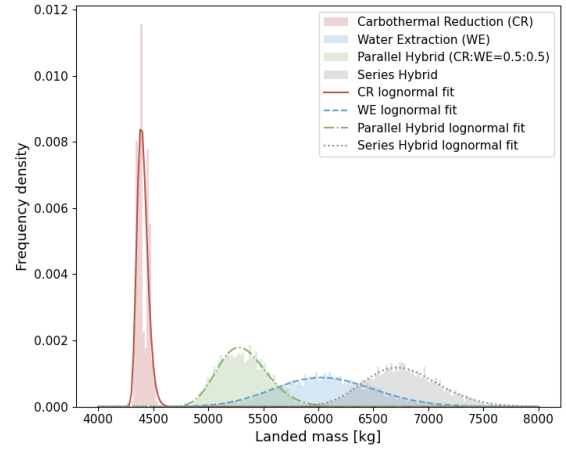


Figure 19: Excavation rate to meet target production, 10 t of LOX and 1.25 t of LH₂. The best case for water ice content distribution: $\mathcal{N}(30, 2^2)$.



(a) Water ice content: $\text{Log-normal}(\ln(4), 0.3^2)$.

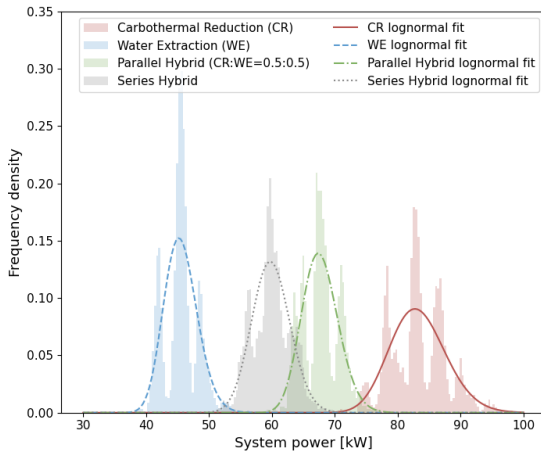
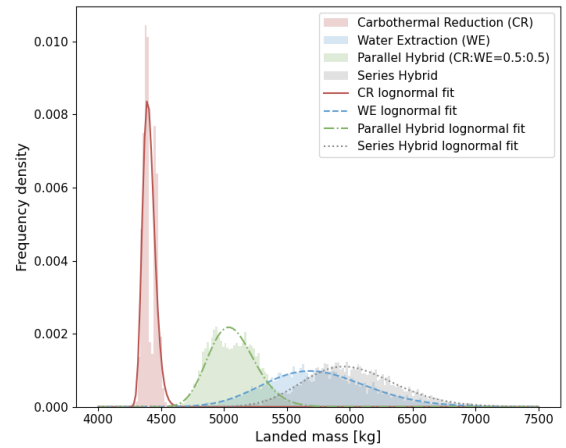


Figure 20: Power consumption to produce 10 t of LOX and 1.25 t of LH₂. The best case for water ice content distribution: $\mathcal{N}(30, 2^2)$.



(b) Water ice content: $\mathcal{N}(30, 2^2)$.

Figure 21: Mass requirement to meet target production of 10 t of LOX and 1.25 t of LH₂.

show similar values. This indicates the required landed mass of these architectures in the worst case could be almost the same.

7. Discussion

7.1. Summary of key findings

As can be seen in Fig. 7a, the CR, architecture appears to be the lightest for one year operation. This result is aligned with what Kleinhenz and Paz concluded [23], although the mass of additional methane mass and its storage due to the imperfect reactant recycling is often overlooked in the literature.

For power consumption, our study shows that the WE architecture can be often the least power-consuming design (Figs. 8, 10, and 13). It should be noted that the CR technology in this paper requires direct thermal power instead of electrical power. This can be particularly challenging for the Series Hybrid architecture since the CR process of this hybrid architecture is conducted in a PSR. This requires a mirror system suggested in [15], indicating more landed mass is required compared to the other architectures.

From the Monte Carlo studies (Sec. 6), the WE architecture turns out to require the largest excavation rate range, highlighting the challenge of engineers to optimize its design. This can also be seen in Fig. 21 as the widest range of the required system mass for the WE plant. Table 5 summarizes

Table 5

Baseline mass and additional mass for the improved robustness.

(a) Water ice content: $Log-normal(\ln(4), 0.3^2)$.

Confidence level to meet the target production	Comparable mass [kg]			
	CR	WE	Parallel	Series
50%	4,406	6,064	5,319	6,762
95%	4,483	6,828	5,707	7,368

(b) Water ice content: $\mathcal{N}(30, 2^2)$.

Confidence level to meet the target production	Comparable mass [kg]			
	CR	WE	Parallel	Series
50%	4,406	5,754	5,072	6,019
95%	4,483	6,493	5,389	7,673

the required mass with a 50% confidence to meet the target production rate and those with a 95% confidence. To improve the robustness of each plant design, 95% confidence is more desirable. The WE architecture requires 750 kg of additional mass to achieve this confidence while the CR architecture only requires about 75 kg.

7.2. Benefits and risks of each plant architecture

7.2.1. Carbothermal reduction architecture

The CR plant can achieve the lowest required excavation rate among the examined architectures (Fig. 17). Moreover, the CR plant can be the lightest architecture when the operational period is one year (Figs. 9a, 11a, and 12a). However, this architecture depends the most on the import of resources from Earth (Fig. 7), which can make it significantly heavier (and costly) when the operational period is longer (Fig. 9b). Another drawback of this architecture is the relatively high power consumption (see e.g., Figs. 10 and 18).

7.2.2. Water extraction architecture

As the Monte Carlo analyses reveals, the WE plant has the widest range in the required regolith excavation rate (Fig. 17). Although it can still be the lightest plant architecture for three years' operation (see, e.g., Figs. 9b and 12b), it requires a lot more mass to improve the robustness of the system (Table 5). If the water content in the excavated regolith is indeed as high as 30 wt% as reported in [38], the expected regolith excavation becomes smaller (Fig. 19) and the expected power consumption also becomes smaller than the other architectures (Fig. 20).

7.2.3. Parallel Hybrid architecture

The performance, indicated by the power consumption, and regolith excavation, of the Parallel Hybrid architecture

turned out to be between that of the CR the WE architectures. The required landed mass for the Parallel Hybrid architecture is not the lightest. However, the mass difference between the Parallel Hybrid architecture and the CR or the WE architecture not always significant (see e.g., Fig. 11b), indicating that one can gather a lot more information that cannot be obtained from the CR or WE architecture by adding a little mass. Therefore, having a hybrid pilot plant to gather more information to help decision-makers make more informed decisions for a full-scale plant could be beneficial. This potential flexibility in the operation and deployment of a hybrid plant should be explored in the future.

7.2.4. Series Hybrid architecture

The obvious benefit of the Series Hybrid architecture is the small regolith excavation rate with a small variance regardless of the water ice content (Figs. 17 and 19). This merit comes with a cost as the required mass which is often the heaviest among the examined architectures. This mass cost can become even larger when we consider the technological challenge of performing the CR process in a PSR.

8. Conclusion

This paper has proposed a new lunar ISRU production plant architecture integrating both carbothermal reduction of dry regolith and water extraction from icy regolith. Two different types of hybrid plants are explored. The Parallel Hybrid architecture has two mining sites in both a PEL and a PSR processing regolith simultaneously. In the Series Hybrid architecture, dry regolith tailing from the water extraction is further processed by carbothermal reduction. The potential

concept of operations of the proposed hybrid architectures is discussed in detail.

The proposed hybrid plant architectures are compared with conventional carbothermal reduction and water extraction plants in terms of mass and power. The total mass and power are estimated from the subsystem-level models of each plant design. Some key parameters that affect the mass and power significantly, such as water ice content, are detected and investigated. Furthermore, Monte Carlo simulations of 5000 scenarios have detected the range of required excavation rate and the power consumption of each plant design.

The uncertainty in water ice content largely affects the required excavation rate. This suggests the urgent need to gather more information on lunar water ice. The Series Hybrid architecture turned out to be a reasonable choice in terms of the regolith excavation rate showing its merit regardless of the water ice content. However, the Series Hybrid architecture becomes the heaviest architecture in many cases.

Although this paper focuses on the plant designs, the potential flexible operations enabled by the proposed hybrid design should be explored further. By gathering more information on both technologies and their operations in the lunar environment, a hybrid pilot plant may provide crucial information for engineers and mission architects. It can help, ultimately, inform better decisions for full-scale plant design and deployment in the coming decades.

Acknowledgement

The authors would like to thank Dr. Joshua N. Rasera and Luka Malone for their reviews and thoughtful suggestions for improvement.

A. Comparisons with existing mass and power estimation

This appendix compares the mass and power of each subsystem estimated from the proposed model with values reported in [7, 23]. Table 6 lists the mass and power of each subsystem estimated using the proposed model and reported in Ref. [7]. Linne et al. scaled their plant using three independent plants with each producing 3.5 t of oxygen. To compare with this model, we scaled a plant to produce 3.5 t of oxygen and multiplied the mass and power by three. There are large differences in the mass of the tanks. This is likely due to the different assumptions in the reactant recycle rate. In our model, only 91% of the reactant is assumed to be recycled, whereas such an assumption is not made in Ref. [7]. Ref. [7] also modeled material transportation and size sorting subsystems in more detail than this paper, which leads to a large mass and power difference in the materials processing and handling subsystem.

Table 7 lists the mass and power of each subsystem estimated using the proposed model and reported in Ref. [23]. To compare these values, the assumptions here are adopted from Ref. [23]. The water content used here is 5 wt%, and the operational availability is adjusted to 225 days per lunar year. The ratio of O₂ and H₂ here is 6:1; therefore, the plant is scaled to produce 13.3 t of LOX and 1.7 t of LH₂. The mass difference in the water extractor is due to the water extraction method; our extractor model is based on a batch operation, whereas Kleinhenz and Paz assumed continuous water extraction [23]. The required number of excavators is one based on our model, which is also different from the two excavators' operation in Ref. [23]. The mass of gas dryers is modeled based on the in-house developed hardware at Johnson Space Center in Ref. [23], which causes large mass difference from the model developed in this paper. There is another large difference in the total mass of water tankers due to the number of tankers. While Kleinhenz and Paz assumed only two tankers are required [23], our model outputs a lighter total mass when 10 tankers are used. This mass can be further lighter by increasing the maximum number of tankers; however, operating a large number of tankers could increase the complexity of the total system.

Table 6
Comparison of the Carbothermal Reduction Plant with Linne et al. [7]

Element	Mass [kg]* ¹		Power [W]* ¹	
	Est. value	Ref. [23]	Est. value	Ref. [23]
CR reactor	448	177	89,828	43,290
Desulfurization	-	78	-	20
Methanation reactor	51	42	-	-
Recycle loop compressor	2	2	204	1,482
Heat exchanger	2	17	-	-
Condenser/electrolyzer H ₂ O tank	-	28	-	-
System gas tank w/ compressor	-	18	-	585
H ₂ tank	192	8	-	-
CH ₄ tank	91	8	-	-
Materials processing & handling	54	350	2	793
Electrolyzer subsystem	13	199	16,274	12,480
Excavator	223	260	633	-

* 1: All values include 30% growth [45].

Table 7
Comparison of the direct water extraction plant with Kleinhenz and Paz [23].

Element	Mass [kg] ^{*1}		Power [kW] ^{*1}	
	Est. value	Ref. [23]	Est. value	Ref. [23]
Water extractor	533	335	25.01	20.75
Excavator	86	160	0.49	0.21
O ₂ liquefaction	169	153	4.08	4.09
O ₂ cryostorage	242	213	-	-
H ₂ liquefaction	1933	1780	25.94	21.17
H ₂ cryostorage	282	299	-	-
H ₂ & O ₂ dryers	1	52	-	0.06
PEM electrolysis	10	48	22.32	22.04
Water tank	264	123	-	0.20
Water tankers	3742	1868	2.63	PEL: 0.38 PSR: 0.53

* 1: All values do not include 30% growth to compare them with Ref. [23].

References

- [1] I. A. Crawford, Lunar resources, *Progress in Physical Geography: Earth and Environment* 39 (2015) 137–167.
- [2] S. O. Starr, A. C. Muscatello, Mars in situ resource utilization: a review, *Planetary and Space Science* 182 (2020) 104824.
- [3] M. Anand, I. Crawford, M. Balat-Pichelin, S. Abanades, W. van Westrenen, G. Péraudeau, R. Jaumann, W. Seboldt, A brief review of chemical and mineralogical resources on the moon and likely initial in situ resource utilization (isru) applications, *Planetary and Space Science* 74 (2012) 42–48. Scientific Preparations For Lunar Exploration.
- [4] L. Schlüter, A. Cowley, Review of techniques for in-situ oxygen extraction on the moon, *Planetary and Space Science* 181 (2020) 104753.
- [5] H. Sargeant, S. Barber, M. Anand, F. Abernethy, S. Sheridan, I. Wright, A. Morse, Hydrogen reduction of lunar samples in a static system for a water production demonstration on the moon, *Planetary and Space Science* 205 (2021) 105287.
- [6] K. A. Lee, L. Oryshchyn, A. Paz, M. Reddington, T. M. Simon, The roxygen project: Outpost-scale lunar oxygen production system development at johnson space center, *Journal of Aerospace Engineering* 26 (2013) 67–73.
- [7] D. L. Linne, J. M. Schuler, L. Sibille, J. E. Kleinhenz, A. J. Colozza, H. J. Fincannon, S. R. Oleson, N. H. Suzuki, L. Moore, Lunar production system for extracting oxygen from regolith, *Journal of Aerospace Engineering* 34 (2021).
- [8] E. Rice, S. Rosenberg, O. Musbah, P. Hermes, P. Bemowski, Carbothermal reduction of lunar materials for oxygen production on the moon, in: 34th Aerospace Sciences Meeting and Exhibit, American Institute of Aeronautics and Astronautics, Reston, Virginia, 1996. doi:10.2514/6.1996-487.
- [9] I. Troisi, P. Lunghi, M. Lavagna, Oxygen extraction from lunar dry regolith: Thermodynamic numerical characterization of the carbothermal reduction, *Acta Astronautica* 199 (2022) 113–124.
- [10] B. White, N. Haggerty, Carbothermal reduction system overview and developments in support of the artemis program and a commercial lunar economy, in: International Conference on Environmental Systems (ICES), 2023.
- [11] J. Prinetto, A. Colagrossi, A. Dottori, I. Troisi, M. R. Lavagna, Terrestrial demonstrator for a low-temperature carbothermal reduction process on lunar regolith simulant: Design and aiv activities, *Planetary and Space Science* 225 (2023) 105618.
- [12] L. Sibille, D. Sadoway, A. Sirk, P. Tripathy, O. Melendez, E. Standish, J. Dominguez, D. Stefanescu, P. Curreri, S. Poizeau, Recent advances in scale-up development of molten regolith electrolysis for oxygen production in support of a lunar base, in: 47th AIAA Aerospace Sciences Meeting including The New Horizons Forum and Aerospace Exposition, 2009. URL: <https://arc.aiaa.org/doi/abs/10.2514/6.2009-659>. doi:10.2514/6.2009-659. arXiv:<https://arc.aiaa.org/doi/pdf/10.2514/6.2009-659>.
- [13] D. Fray, Anodic and cathodic reactions in molten calcium chloride, *Canadian Metallurgical Quarterly* 41 (2002) 433–439.
- [14] K. Ono, R. Suzuki, A new concept for producing ti sponge: Calciothermic reduction, *JOM* 54 (2002) 59–61.
- [15] G. F. Sowers, C. B. Dreyer, Ice mining in lunar permanently shadowed regions, *New Space* 7 (2019) 235–244.
- [16] T. M. Pelech, G. Roesler, S. Saydam, Technical evaluation of off-earth ice mining scenarios through an opportunity cost approach, *Acta Astronautica* 162 (2019) 388–404.
- [17] C. Purrington, G. Sowers, C. Dreyer, Thermal mining of volatiles in lunar regolith simulant, *Planetary and Space Science* 222 (2022) 105550.
- [18] G. L. Schieber, B. M. Jones, T. M. Orlando, P. G. Loutzenhiser, Indirect solar receiver development for the thermal extraction of h₂o(v) from lunar regolith: Heat and mass transfer modeling, *Acta Astronautica* 190 (2022) 365–376.
- [19] L. He, C. Wang, G. Zhang, Y. Pang, W. Yao, A novel auger-based system for extraterrestrial in-situ water resource extraction, *Icarus* 367 (2021) 114552.
- [20] Y. Liu, C. Wang, Y. Pang, Q. Wang, Z. Zhao, T. Lin, Z. Wang, T. Shen, S. Liu, J. Song, X. Lai, X. Quan, W. Yao, Water extraction from icy lunar regolith by drilling-based thermal method in a pilot-scale unit, *Acta Astronautica* 202 (2023) 386–399.
- [21] J. Collins, K. R. Araghi, Lunar water extraction via lunar auger dryer isru (ladi), in: ASCEND 2023, American Institute of Aeronautics and Astronautics, Reston, Virginia, 2023. doi:10.2514/6.2023-4758.
- [22] L. Kiewiet, N. M. Hab, F. M. Marchese, R. Freer, P. Zabel, Trade-off and optimization for thermal lunar water extraction system, in: 73rd International Astronautical Congress (IAC), 2022. URL: <https://dl.iafastro.directory/event/IAC-2022/paper/68956/>.
- [23] J. E. Kleinhenz, A. Paz, Case studies for lunar ISRU systems utilizing polar water, in: ASCEND 2020, American Institute of Aeronautics and Astronautics, Reston, Virginia, 2020. doi:10.2514/6.2020-4042.
- [24] J. D. Cole, S. Lim, H. M. Sargeant, S. Sheridan, M. Anand, A. Morse, Water extraction from icy lunar simulants using low power microwave heating, *Acta Astronautica* 209 (2023) 95–103.
- [25] L. A. Taylor, W. D. Carrier, Production of oxygen on the moon: Which processes are best and why, *AIAA Journal* 30 (1992) 2858–2863.
- [26] J. E. Kleinhenz, A. Paz, An ISRU propellant production system for a fully fueled mars ascent vehicle, in: 10th Symposium on Space Resource Utilization, American Institute of Aeronautics and Astronautics, Reston, Virginia, 2017. doi:10.2514/6.2017-0423.
- [27] H. Chen, T. Du Sarton Jonchay, L. Hou, K. Ho, Integrated in-situ resource utilization system design and logistics for mars exploration, *Acta Astronautica* 170 (2020) 80–92.
- [28] K. Hadler, D. Martin, J. Carpenter, J. J. Cilliers, A. Morse, S. Starr, J. N. Rasera, K. Seweryn, P. Reiss, A. Meurisse, A universal framework for space resource utilisation (SRU), *Planetary and Space Science* 182 (2020) 104811.
- [29] L. R. Gaddis, K. H. Joy, B. J. Bussey, J. D. Carpenter, I. A. Crawford, R. C. Elphic, J. S. Halekas, S. J. Lawrence, L. Xiao, Recent Exploration of the Moon: Science from Lunar Missions Since 2006, *Reviews in Mineralogy and Geochemistry* 89 (2023) 1–51.
- [30] J. J. Cilliers, J. N. Rasera, K. Hadler, Estimating the scale of space resource utilisation (SRU) operations to satisfy lunar oxygen demand, *Planetary and Space Science* 180 (2020) 104749.
- [31] J. Cilliers, K. Hadler, J. Rasera, Toward the utilisation of resources in space: knowledge gaps, open questions, and priorities, *npj Microgravity* 9 (2023).

- [32] F. J. Guerrero-Gonzalez, P. Zabel, System analysis of an ISRU production plant: Extraction of metals and oxygen from lunar regolith, *Acta Astronautica* 203 (2023) 187–201.
- [33] E. Santiago-Maldonado, D. L. Linne, ISRU System Model Tool: From Excavation to Oxygen Production, Technical Report, 2007.
- [34] Y. Takubo, H. Chen, K. Ho, Hierarchical reinforcement learning framework for stochastic spaceflight campaign design, *Journal of Spacecraft and Rockets* 59 (2022) 421–433.
- [35] L. Malone, M.-A. Cardin, J. Cilliers, K. Hadler, Development of a comprehensive lunar mining simulator to study design and decision-making under uncertainty, in: 73rd International Astronautical Congress (IAC), 2022.
- [36] A. Colaprete, P. Schultz, J. Heldmann, D. Wooden, M. Shirley, K. Ennico, B. Hermalyn, W. Marshall, A. Ricco, R. C. Elphic, D. Goldstein, D. Summy, G. D. Bart, E. Asphaug, D. Korycansky, D. Landis, L. Sollitt, Detection of water in the Icarus ejecta plume, *Science (New York, N.Y.)* 330 (2010) 463–468.
- [37] P. O. Hayne, A. Hendrix, E. Sefton-Nash, M. A. Siegler, P. G. Lucey, K. D. Retherford, J.-P. Williams, B. T. Greenhagen, D. A. Paige, Evidence for exposed water ice in the moon's south polar regions from lunar reconnaissance orbiter ultraviolet albedo and temperature measurements, *Icarus* 255 (2015) 58–69.
- [38] S. Li, P. G. Lucey, R. E. Milliken, P. O. Hayne, E. Fisher, J.-P. Williams, D. M. Hurley, R. C. Elphic, Direct evidence of surface exposed water ice in the lunar polar regions, *Proceedings of the National Academy of Sciences of the United States of America* 115 (2018) 8907–8912.
- [39] E. Mazarico, G. A. Neumann, D. E. Smith, M. T. Zuber, M. H. Torrence, Illumination conditions of the lunar polar regions using lola topography, *Icarus* 211 (2011) 1066–1081.
- [40] A. Zuniga, H. Modi, A. Kaluthantrige, H. Vertadier, Building an economical and sustainable lunar infrastructure to enable human lunar missions, in: 70th International Astronautical Congress (IAC), 2019. URL: <https://dl.iafaastro.directory/event/IAC-2019/paper/54311/>.
- [41] P. O. Hayne, O. Aharonson, N. Schörghofer, Micro cold traps on the moon, *Nature Astronomy* 5 (2021) 169–175.
- [42] D. Kaschubek, M. Killian, L. Grill, System analysis of a moon base at the south pole: Considering landing sites, ECLSS and ISRU, *Acta Astronautica* 186 (2021) 33–49.
- [43] S. Sathyan, M. Bhatt, M. Chowdhury, P. Gläser, D. Misra, N. Srivastava, S. Narendranath, K. S. Sajinkumar, A. Bhardwaj, Potential landing sites characterization on lunar south pole: De-gerlache to shackleton ridge region, *Icarus* (2024) 115988.
- [44] G. B. Sanders, W. C. Carey, J.-C. Piedboeuf, A. Lorenzoni, Lunar in-situ resource utilization in the isecg human lunar exploration reference architecture, in: 61st International Astronautical Congress (IAC), 2010.
- [45] American Institute of Aeronautics and Astronautics, American national standard: Mass properties control for space systems, ??? URL: <https://webstore.ansi.org/standards/aiaa/ansiaiaa120a2015>.
- [46] P. O. Hayne, J. L. Bandfield, M. A. Siegler, A. R. Vasavada, R. R. Ghent, J.-P. Williams, B. T. Greenhagen, O. Aharonson, C. M. Elder, P. G. Lucey, D. A. Paige, Global regolith thermophysical properties of the moon from the diviner lunar radiometer experiment, *Journal of Geophysical Research: Planets* 122 (2017) 2371–2400.
- [47] C. Schwandt, J. A. Hamilton, D. J. Fray, I. A. Crawford, The production of oxygen and metal from lunar regolith, *Planetary and Space Science* 74 (2012) 49–56. Scientific Preparations For Lunar Exploration.
- [48] L. A. Taylor, C. Pieters, A. Patchen, D.-H. S. Taylor, R. V. Morris, L. P. Keller, D. S. McKay, Mineralogical and chemical characterization of lunar highland soils: Insights into the space weathering of soils on airless bodies, *Journal of Geophysical Research: Planets* 115 (2010).
- [49] F. J. Guerrero-Gonzalez, ISRU Lib documentation site, 2023. URL: <https://wiki.tum.de/display/lpe/ISRUlib>.
- [50] R. J. Gustafson, Carbon reduction of lunar regolith for oxygen production, in: AIP Conference Proceedings, AIP, 2005, pp. 1224–1228. doi:10.1063/1.1867249.
- [51] M. Samouhos, P. Tsakiridis, M. Iskander, M. Taxiarchou, K. Betsis, In-situ resource utilization: ferrosilicon and sic production from bp-1 lunar regolith simulant via carbothermal reduction, *Planetary and Space Science* 212 (2022) 105414.
- [52] R. Balasubramaniam, S. Gokoglu, U. Hegde, The reduction of lunar regolith by carbothermal processing using methane, *International Journal of Mineral Processing* 96 (2010) 54–61.
- [53] H.-C. Lee, S. Dhage, M. S. Akhtar, D. H. Kwak, W. J. Lee, C.-Y. Kim, O.-B. Yang, A simulation study on the direct carbothermal reduction of SiO_2 for Si metal, *Current Applied Physics* 10 (2010) S218–S221.
- [54] R. Woods-Robinson, M. A. Siegler, D. A. Paige, A model for the thermophysical properties of lunar regolith at low temperatures, *Journal of Geophysical Research: Planets* 124 (2019) 1989–2011.
- [55] S. J. Keihm, Interpretation of the lunar microwave brightness temperature spectrum: Feasibility of orbital heat flow mapping, *Icarus* 60 (1984) 568–589.
- [56] S. S. Schreiner, J. A. Dominguez, L. Sibille, J. A. Hoffman, Thermophysical property models for lunar regolith, *Advances in Space Research* 57 (2016) 1209–1222.
- [57] A. Muscatello, R. Gustafson, Comparison of direct solar energy to resistance heating for carbothermal reduction of regolith, in: 49th AIAA Aerospace Sciences Meeting including the New Horizons Forum and Aerospace Exposition, American Institute of Aeronautics and Astronautics, Reston, Virginia, 2011. doi:10.2514/6.2011-699.
- [58] C. J. Cremers, H. S. Hsia, Thermal conductivity of Apollo 16 lunar fines, *Lunar and Planetary Science Conference Proceedings* 3 (1974) 2703–2708.
- [59] L. Schrenk, Development of an In-Situ Resource Utilization (ISRU) Module for the Analysis Environment HabNet, M.Sc. Thesis, Technical University of Munich, 2015.
- [60] C. Junaedi, K. Hawley, D. Walsh, S. Roychoudhury, M. B. Abney, J. L. Perry, CO_2 reduction assembly prototype using microlith-based sabatier reactor for ground demonstration, 44th International Conference on Environmental Systems, 2014.
- [61] U. Hegde, R. Balasubramaniam, S. Gokoglu, Analysis of water extraction from lunar regolith, in: 50th AIAA Aerospace Sciences Meeting including the New Horizons Forum and Aerospace Exposition, 2012. URL: <https://arc.aiaa.org/doi/abs/10.2514/6.2012-634>. doi:10.2514/6.2012-634. arXiv:<https://arc.aiaa.org/doi/pdf/10.2514/6.2012-634>.
- [62] R. P. Mueller, J. D. Smith, J. M. Schuler, A. J. Nick, N. J. Gelino, K. W. Leucht, I. I. Townsend, A. G. Dokos, Design of an excavation robot: Regolith advanced surface systems operations robot (rassor) 2.0, in: R. B. Malla, J. H. Agui, P. J. van Susante (Eds.), *Earth and Space 2016*, American Society of Civil Engineers, Reston, VA, 2016, pp. 163–174.

doi:10.1061/9780784479971.018.

- [63] L. A. Haas, S. E. Khalafalla, Effect of physical parameters on the reaction of graphite with silica in vacuum, ??? URL: <https://ntrs.nasa.gov/api/citations/19690004119/downloads/19690004119.pdf>.
- [64] F. Schuster, ISRU Lib: Parametric Analytical Modeling of H₂/O₂ Electrolysis, Liquefaction and Cryostorage, Bachelor Thesis, Technical University of Munich, 2023.
- [65] A. Dottori, I. Troisi, M. Lavagna, s. Pirrotta, F. Latini, Lunar pilot plant payload design toward in situ demonstration of oxygen extraction by carbothermal reduction, 2023. doi:10.13009/EUCASS2023-283.
- [66] L. Schlüter, A. Cowley, Y. Pennec, M. Roux, Gas purification for oxygen extraction from lunar regolith, *Acta Astronautica* 179 (2021) 371–381.
- [67] F. E. Meyen, M. H. Hecht, J. A. Hoffman, Thermodynamic model of mars oxygen isru experiment (moxie), *Acta Astronautica* 129 (2016) 82–87.
- [68] Electrolyzer Exergy Analysis for an Environmental Control and Life Support System, volume Volume 6A: Energy of *ASME International Mechanical Engineering Congress and Exposition*, 2018. URL: <https://doi.org/10.1115/IMECE2018-88119>. doi:10.1115/IMECE2018-88119.
- [69] M. Sakurai, Y. Sone, T. Nishida, H. Matsushima, Y. Fukunaka, Fundamental study of water electrolysis for life support system in space, *Electrochimica Acta* 100 (2013) 350–357.
- [70] Ö. Akay, A. Bashkatov, E. Coy, K. Eckert, K. E. Einarsrud, A. Friedrich, B. Kimmel, S. Loos, G. Mutschke, L. Röntzsch, M. D. Symes, X. Yang, K. Brinkert, Electrolysis in reduced gravitational environments: current research perspectives and future applications, *NPJ microgravity* 8 (2022) 56.
- [71] W. L. Johnson, D. M. Hauser, D. W. Plachta, X.-Y. Wang, B. F. Banker, P. S. Desai, J. R. Stephens, A. M. Swanger, Comparison of oxygen liquefaction methods for use on the martian surface, *Cryogenics* 90 (2018) 60–69.
- [72] M. Lavagna, A. Dottori, I. Troisi, A. Colagrossi, J. Prinetto, Solid-gas carbothermal reduction for water production from lunar regolith simulant: Experimental results, in: *European Lunar Symposium*, 2023. URL: https://www.youtube.com/watch?v=jm-0_k2nsJc.
- [73] D. Deserranno, M. Zagarola, X. Li, S. Mustafi, Optimization of a brayton cryocooler for zbo liquid hydrogen storage in space, *Cryogenics* 64 (2014) 172–181.
- [74] R. L. Korotev, B. L. Jolliff, R. A. Zeigler, J. J. Gillis, L. A. Haskin, Feldspathic lunar meteorites and their implications for compositional remote sensing of the lunar surface and the composition of the lunar crust, *Geochimica et Cosmochimica Acta* 67 (2003) 4895–4923.
- [75] K. M. Cannon, A lunar soil classification system for space resource utilization, *Planetary and Space Science* 237 (2023) 105780.
- [76] J. C. Graf, Lunar soils grain size catalog, ??? URL: <https://ntrs.nasa.gov/citations/19930012474>.
- [77] W. I. Ridley, A. M. Reid, J. L. Warner, R. W. Brown, R. Gooley, C. Donaldson, Glass compositions in apollo 16 soils 60501 and 61221, in: *4th Lunar and Planetary Science Conference*, volume 4, 1973, p. 309. URL: <https://ui.adsabs.harvard.edu/abs/1973LPSC...4..309R>.
- [78] M. T. Zuber, J. W. Head, D. E. Smith, G. A. Neumann, E. Mazarico, M. H. Torrence, O. Aharonson, A. R. Tye, C. I. Fassett, M. A. Rosenburg, H. J. Melosh, Constraints on the volatile distribution within shackleton crater at the lunar south pole, *Nature* 486 (2012) 378–381.
- [79] K. M. Cannon, D. T. Britt, A geologic model for lunar ice deposits at mining scales, *Icarus* 347 (2020) 113778.